

Topological Operations Around Exceptional Points via Shortcuts to Adiabaticity

Vishnu Chavva¹ and Hugo Ribeiro¹

¹*Department of Physics and Applied Physics, University of Massachusetts Lowell, Lowell, MA 01854, USA*

The existence of singularities in the spectrum of non-Hermitian Hamiltonians leads to a non-trivial spectral topology which can be exploited to generate topological operations. However, their implementation has remained elusive due to the difficulty of generating a true adiabatic evolution. Here, we develop fast, robust control protocols that generate a desired topological operation. Our strategy relies on shortcuts to adiabaticity, but is not a trivial extension. The presence of spectral singularities renders the strategy developed for Hermitian Hamiltonians impractical as it will lead to faulty control protocols. Moreover, due to the dynamics sensitivity to parameter uncertainties, not all shortcuts to adiabaticity can be used in a realistic setting. We illustrate our method in the context of a two-mode non-Hermitian Hamiltonian and discuss why in general celebrated shortcuts to adiabaticity like transitionless driving and superadiabatic transitionless are not appropriate control protocols for non-Hermitian systems.

I. INTRODUCTION

One of the fundamental postulates of quantum mechanics is that closed systems are described by Hermitian Hamiltonians ($\hat{H} = \hat{H}^\dagger$). This guarantees a real spectrum for \hat{H} and ensures that the evolution operators obtained by solving Schrödinger's equation are unitary and probability is conserved. However, most physical systems are best modeled by assuming that they exchange energy with a large environment. A straightforward way of modeling such dissipative systems is through the use of non-Hermitian (NH) Hamiltonians ($\hat{H} \neq \hat{H}^\dagger$) (see Fig. 1).

Theories based on NH Hamiltonians have been successful in describing photonic systems exhibiting gain/loss [1–3], interactions between atomic systems and their environment [4–6], and non-equilibrium dynamics present in condensed matter systems [7–9]. The unique properties of these NH Hamiltonians have, and continue to be, the driving force behind their growing theoretical and experimental interest [10–13].

A signature feature of NH Hamiltonians is their complex spectrum. Generally, the real part of the spectrum corresponds to the system energy while the imaginary part accounts for the dissipative behavior. If the NH Hamiltonian depends on externally controllable parameters, one can tune the interplay between dissipative and coherent dynamics. Furthermore, for certain parameter values, eigenvalues and eigenvectors coalesce [3, 11, 14–17], and the NH Hamiltonian cannot be diagonalized. These singularities in parameter space are known as exceptional points (EPs) and give rise to a non-trivial spectral topology [18–20].

The archetypal characteristic is a spectrum that does not return to itself when the parameters are varied along a closed contour (in parameter space) that encircles an EP. Eigenvalues appear to “swap” with one another, forming a so-called eigenvalue braid. This topological behavior is appropriately referred to as eigenvalue braiding [21–23], and constitutes much of the interest in this work. Additionally, as the eigenvalues braid, the eigen-

vectors acquire an invariant topological phase, determined by the dimensions of the NH Hamiltonian [24–27].

Realizing eigenvalue braiding, however, is a cumbersome process since only one eigenstate (the least damped eigenstate) follows adiabatic evolution [28–33]. Thus, initializing an instantaneous eigenstates of a non-Hermitian and “slowly” varying its parameters does not generate an evolution that guarantees eigenvalue braiding [34–36].

In this work, we present a highly general strategy to design fast, robust control protocols that generate eigenvalue braiding for NH systems. Our approach takes inspiration from the field of shortcuts-to-adiabaticity (STAs) [37–42], specifically the dressed state method [43, 44]. While it would appear that extending the dressed state method to NH Hamiltonians would be a straightforward generalization, the non-trivial spectral topology of NH Hamiltonians, and in particular the presence of singularities, prohibits one from following the framework developed for Hermitian Hamiltonians. Doing so will lead to control protocols that fail to mimic the desired adiabatic evolution.

Moreover, and in stark contrast to Hermitian STAs, non-Hermitian STAs do not inherit the robustness of the original adiabatic protocol against parameter uncertainties. This follows from the violation of the adiabatic theorem for NH Hamiltonians. Our work shows how to construct adequate dressed states that allow one to find robust, experimentally realizable control schemes. Our method is independent of a particular choice of contour in parameter space and, much like the Hermitian dressed state method, offers considerable freedom to design protocols that obey the constraints of specific platforms.

Extending STAs to NH Hamiltonians is not a new idea. Several works [45, 46] have already discussed how to realize transitionless driving (TD) [37, 39] in the context of NH Hamiltonians. However, these work do not discuss how to restore adiabaticity around EPs nor the robustness of the non-Hermitian TD against parameter uncertainties. Parameter uncertainties effectively lead to transitions between (unperturbed) eigenstates, including

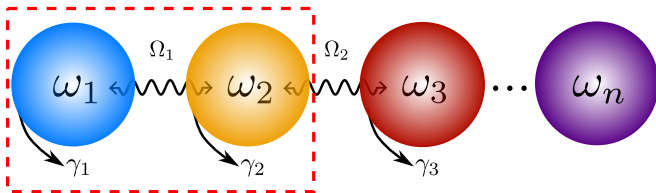


Figure 1. N -coupled modes with local dissipation. The dissipative evolution of the system can be described by an effective non-Hermitian Hamiltonian with corresponding coupling strengths Ω_n and dissipation rates γ_n .

transitions to the least damped eigenstate. Populating the latter will unavoidably result in its preparation at the end of the protocol, independently of which eigenstate was initially prepared [47]. More recently, two works [48, 49] showed that there exists a special choice of closed contour around an EP that allows one to generate adiabatic evolution akin to that of Hermitian systems. While the strategy allows one to realize and study adiabatic passage with NH Hamiltonians, it remains constrained to one specific class of trajectories. As we discuss, our method is not restricted by a choice of initial contour. This allows one to explore adiabatic phenomena around EPs without being limited to a single type of evolution.

The remainder of this paper is organized as follows: In Sec. II we discuss how singularities in the spectrum of NH Hamiltonians must be handled to define valid STAs and how the resulting framework fundamentally differs from Hermitian STAs. In Sec. III, we apply our formalism to a two-mode system to illustrate the differences between the Hermitian and non-Hermitian case, to discuss the issue of robustness, and to advance NH STAs that are both robust against parameter uncertainties and experimentally feasible.

II. PRELIMINARIES

A. Spectral flow and topological operations

We consider the generic N -dimensional non-Hermitian Hamiltonian

$$\hat{H} = \hat{H}(\mathbf{p}), \quad (1)$$

where $\mathbf{p} = (p_1, \dots, p_n) \in \mathbb{R}^n$ is a shorthand notation to indicate that \hat{H} depends on n parameters that can be externally varied. The right eigenstates of Eq. (1) and corresponding right eigenvalues are defined by

$$\hat{H}(\mathbf{p})|\psi_j(\mathbf{p})\rangle = \lambda_j(\mathbf{p})|\psi_j(\mathbf{p})\rangle. \quad (2)$$

Generically, as one varies \mathbf{p} , the spectrum $\text{Sp}[\hat{H}(\mathbf{p})] = \{\lambda(\mathbf{p}) | \det[\hat{H}(\mathbf{p}) - \lambda(\mathbf{p})\mathbb{1}] = 0\} \equiv \{\lambda_j(\mathbf{p})\}_{j=1}^N$ becomes degenerate at singularities known as exceptional points of

order k (EP $_k$), with $2 \leq k \leq N$ [14, 50]. At these degeneracy points k eigenvalues and eigenstates coalesce and \hat{H} becomes non-diagonalizable. Since the eigenvalues of a non-Hermitian Hamiltonian are in general complex (the spectrum of \hat{H} can be entirely real, if parity-time symmetry is respected [51–53]), an EP $_k$ formally corresponds to a branch point (endpoint of a branch cut) associated to the function $\lambda_j : \mathbb{R}^n \rightarrow \mathbb{C}$, $\mathbf{p} \mapsto \lambda_j(\mathbf{p})$ [10].

We label the position in parameter space of the l th EP $_k$ by $\mathbf{p}_{k,l}$ and define $B_k = \{\mathbf{p}_{k,l}\}_{l=1}^L$ as the parameter subspace formed by all EP $_k$'s. The union of all B_k 's forms the parameter space $B_{\text{deg}} = \cup_k B_k$ where the spectrum of Eq. (1) is degenerate. We denote the complement of B_{deg} as $B_{\text{ng}} = B_{\text{deg}}^c$, which corresponds to the parameter space where the spectrum is non-degenerate. The images of $B_k \forall k$ and B_{ng} under the action of $\text{Sp}[\hat{H}(\mathbf{p})]$ define topological manifolds that are in general non-trivial [19–21, 52, 54–57], and which we denote as $\text{Sp}(B_k)$ and $\text{Sp}(B_{\text{ng}})$, respectively.

The non-trivial topology of $\text{Sp}(B_{\text{ng}})$ becomes apparent when one studies how the spectrum varies along a family of closed contours (loops) with a same basepoint. We denote such a family of loops by $\gamma_s[\mathbf{p}(\varepsilon)] \subset B_{\text{ng}}$ with $\varepsilon \in [0, 1]$. Since any loop γ_s starts and ends at the same basepoint, we have $\hat{H}[\gamma_s(\varepsilon = 0)] = \hat{H}[\gamma_s(\varepsilon = 1)]$ and therefore the spectrum must return to itself at the end of the loop. However, it might do so in a non-trivial fashion according to

$$\lambda_j[\mathbf{p}(\varepsilon = 0)] \rightarrow \lambda_j[\mathbf{p}(\varepsilon = 1)] = \lambda_{\sigma(j)}[\mathbf{p}(\varepsilon = 0)], \quad (3)$$

where $\sigma_n(j)$ is one of $1 \leq n \leq N!$ permutations acting on the set $\{1, \dots, j, \dots, N\}$, and which is solely determined by the choice of loop γ_s .

Pairs of loops that are homotopic (can be continuously deformed into one another) in B_{ng} will lead to the same permutation σ_n . By defining $\pi_1(B_{\text{ng}})$ as the set of homotopy equivalence classes of loops and considering the concatenation of loops as a binary operation on $\pi_1(B_{\text{ng}})$, we can make $\pi_1(B_{\text{ng}})$ into a group called the fundamental group [58]. Each element of π_1 corresponds to a unique permutation σ_n and the group operation between two elements of π_1 is associated to the composition of permutations.

To understand how to characterize the elements of $\pi_1(B_{\text{ng}})$, it is useful to consider the image of a loop under the action of $\text{Sp}[\gamma(\mathbf{p})] = \{\lambda_j[\mathbf{p}(\varepsilon)]\}_{j=1}^N$. This produces a contour on $\text{Sp}(B_{\text{ng}})$ that formally corresponds to a braid of N strands [see Fig. 2(a)], commonly known as an eigenvalue braid [18, 22, 35, 59, 60]. Since $\text{Sp}[\gamma(\mathbf{p})]$ defines an isotopy equivalence class of braids (pairs of braids are isotopic, if they can be continuously deformed into one another while keeping the end points fixed and the strands from intersecting) and one can concatenate braids, we can define a group whose elements are equivalence classes of braids with N strands. This group is known as the Artin group B_N [61]. An element of B_N corresponds to an element of $\pi_1(B_{\text{ng}})$, since two isotopic

braids arise from two homotopic loops γ . This implies $\pi_1(B_{\text{ng}}) \cong B_N$.

Since braid concatenation is in general not a commutative operation, one can generate braids belonging to different isotopy classes by concatenating two same loops in a different order. This allows one to represent eigenvalue braiding as a permutation operation defined by

$$\hat{P}_{\sigma_n} = \sum_{j=1}^N \exp[i\beta_{\sigma_n(j),j}] |\psi_{\sigma_n(j)}[\mathbf{p}(\varepsilon=0)]\rangle \langle \psi_j[\mathbf{p}(\varepsilon=0)]|, \quad (4)$$

and which in general fulfills the condition $[\hat{P}_{\sigma_n}, \hat{P}_{\sigma_m}] \neq 0$, if $\sigma_n \neq \sigma_m$. Generating operations that correspond to \hat{P}_{σ} to control a system would be beneficial, as these operations are robust against imprecisions always present in control schemes, e.g., amplitude and phase of driving fields.

B. “Adiabatic” Evolution and Holomorphic Change of Frame Operators

Generating a topological operation corresponding to a particular \hat{P}_{σ_j} requires adiabatically evolving the system by varying \hat{H} along a control loop γ that varies in time. Assuming the equation of motion to be linear and recasting it in the form of a Schrödinger equation, we have that the flow operator $\hat{\Phi}(t)$ [equivalent to the unitary evolution operator $\hat{U}(t)$] obeys

$$i\partial_t \hat{\Phi}(t) = \hat{H}(t) \hat{\Phi}(t), \quad (5)$$

with $\hat{\Phi}(0) = \mathbb{1}$. The flow $\hat{\Phi}(t)$ allows one to find the state of the system at time t , if one knows the state at time $t=0$ through the relation $|k(t)\rangle = \hat{\Phi}(t)|k(0)\rangle$. The problem now is to engineer an $\varepsilon(t)$ such that $\hat{H}\{\gamma[\varepsilon(t/t_f)]\}$ generates an adiabatic dynamics leading to $\hat{\Phi}(t_f) = \hat{P}_{\sigma}$. This is, however, impossible since it has been shown that systems governed by a non-Hermitian Hamiltonian violate the adiabatic theorem [22, 35, 62, 63].

This is best understood in the frame of instantaneous eigenstates (adiabatic frame), where $\hat{H}(t)$ is diagonal at each instant of time t . In the adiabatic frame, the non-Hermitian Hamiltonian governing the dynamics is given by

$$\begin{aligned} \hat{H}_{\text{ad}}(t) &= \hat{S}_{\text{ad}}^{-1}(t) \hat{H}(t) \hat{S}_{\text{ad}}(t) - i \hat{S}_{\text{ad}}^{-1}(t) \partial_t \hat{S}_{\text{ad}}(t) \\ &= \sum_j \lambda_j(t) |\psi_j\rangle \langle \psi_j| - i \hat{S}_{\text{ad}}^{-1}(t) \sum_{j=1}^n \frac{\partial \hat{S}_{\text{ad}}(t)}{\partial \mathbf{p}_j} \hat{\mathbf{p}}_j(t), \end{aligned} \quad (6)$$

where we use Newton’s notation for time differentiation, $\dot{x}(t) = dx(t)/dt$ and

$$\hat{S}_{\text{ad}}[\mathbf{p}(t)] = \sum_{j=1}^n |\psi_j[\mathbf{p}(t)]\rangle \langle \psi_j|. \quad (7)$$

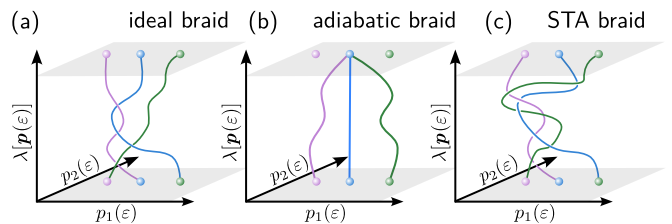


Figure 2. Schematic representations of the eigenvalues braids traced by a choice of contour $\gamma[\mathbf{p}(\varepsilon)]$ with $\mathbf{p} = (p_1, p_2)$. (a) Ideal braid obtained from spectral flow. (b) Adiabatic evolution of eigenstates does not yield the desired eigenvalue braiding. (c) STAs do not in general produce the ideal braid, but still lead to the desired topological operation.

is the time-dependent change of frame operator leading to $\hat{S}_{\text{ad}}^{-1}(t) \hat{H}(t) \hat{S}_{\text{ad}}(t)$ being diagonal.

Since Eq. (7) is explicitly time-dependent (the instantaneous eigenstates of \hat{H} are not stationary), the non-Hermitian Hamiltonian in the adiabatic frame picks up a non-inertial term, which couples the instantaneous eigenstates [see Eq. (6)]. This coupling leads to transitions between the instantaneous eigenstates, which in contrast to the Hermitian case, prevent the system from following adiabatic dynamics even in the long-time limit [see Fig. 2(b)], i.e., when $t_f \rightarrow \infty$. The violation of the adiabatic theorem for non-Hermitian systems has been observed experimentally, particularly in two-mode systems [2, 64–70].

Additionally, to correctly define Eq. (6) one must construct a change of frame operator $\hat{S}_{\text{ad}}(t)$ that is holomorphic everywhere except at the location of the EPs. This is necessary since Eq. (6) requires one to calculate the partial derivative of $\hat{S}_{\text{ad}}(\mathbf{p})$ with respect to the parameters that define the contour, which is only possible if the matrix elements of $\hat{S}_{\text{ad}}(\mathbf{p})$ are holomorphic functions.

It is always possible to construct a holomorphic change of frame operator by first defining the eigenvalues $\lambda_j(t)$ on their associated Riemann surface [71] and then solving for the eigenstates $|\psi_j[\mathbf{p}(t)]\rangle$, which define Eq. (7). We show an explicit example of this procedure in Sec. III.

C. Dressed State Approach to Non-Hermitian Shortcuts-to-Adiabaticity

Now that we have laid down the fundamental concepts allowing one to find the correct representation of any time-dependent non-Hermitian operator in the adiabatic frame, we can formulate a theory to construct non-Hermitian STAs.

Our approach builds on the ideology of the dressed state approach for Hermitian systems [43]: If one is only interested in the topological operation generated by encircling an EP with a control loop $\gamma[\mathbf{p}(t)]$ of duration $t = t_0$, then it is not necessary to follow the ideal adiabatic evolution at all times. It is sufficient to generate an

evolution that only resembles the adiabatic evolution at the initial $t = 0$ and final time $t = t_0$. In other words, we ensure only that the end points of the eigenvalue braids generated by the STA correspond to the end points of the ideal eigenvalue braids [see Fig. 2(c)].

Like for Hermitian systems, we must (1) choose a dressing transformation $\hat{S}_{\text{dr}}(t)$ for the instantaneous eigenstates which vanishes at $t = 0$ and $t = t_0$, and (2) find the associated non-Hermitian control Hamiltonian $\hat{W}(t)$ such that the modified non-Hermitian Hamiltonian $\hat{H}_{\text{mod}}(t) = \hat{H}(t) + \hat{W}(t)$ generates the desired evolution at $t = t_0$. In addition to these requirements, we must introduce a new constraint: (3) the change of frame operators must be holomorphic functions along $\gamma(t)$, otherwise the non-Hermitian STAs will be unusable.

A generic dressing transformation can be parametrized by

$$\hat{S}_{\text{dr}}[\mathbf{p}(t)] = \sum_{j=1}^n |\phi_j[\mathbf{p}(t)]\rangle\langle\phi_j|, \quad (8)$$

where $|\phi_j\rangle$ are the dressed eigenstates. With this parametrization condition (1) implies that Eq. (8) must satisfy

$$\hat{S}_{\text{dr}}(0) = \hat{S}_{\text{dr}}(t_0) = \mathbb{1}. \quad (9)$$

This guarantees that the dressed states coincide with the instantaneous eigenstates $|\psi_j\rangle$ at $t = 0$ and $t = t_0$. This is equivalent to saying that $\hat{W}(t) = 0$ at the end points, which implies that the spectrum of $\hat{H}_{\text{mod}}(t)$ reduces to the spectrum of $\hat{H}(t)$ at $t = 0$ and $t = t_0$.

In the dressed frame, the dynamics is described by the non-Hermitian Hamiltonian

$$\hat{H}_{\text{dr}}(t) = \hat{S}_{\text{dr}}^{-1}(t)\hat{H}_{\text{ad}}(t)\hat{S}_{\text{dr}}(t) - i\hat{S}_{\text{dr}}^{-1}(t)\partial_t\hat{S}_{\text{dr}}(t). \quad (10)$$

By imposing

$$\langle\phi_j|\hat{H}_{\text{dr}}(t)|\phi_i\rangle = 0 \quad (11)$$

for all $i \neq j$ allows one to find the matrix element of the control operator $\hat{W}(t)$.

Since the dressing transformation is explicitly time-dependent, $\hat{H}_{\text{dr}}(t)$ also contains a non-inertial term [see Eq. (10)] obtained from the derivative of $\hat{S}_{\text{dr}}(t)$. To obtain the correct non-inertial term, which defines $\hat{W}(t)$ [see Eq. (11)], one must construct a dressing transformation which is holomorphic along $\gamma(t)$. Therefore, one can see the necessity of including requirement (3) in defining the criteria for a non-Hermitian STA.

As we discuss in Sec. III F, this leads to substantial differences between the Hermitian and non-Hermitian case. In the Hermitian case, any choice of dressing can be viewed as a family of transformations labeled by the loop time t_0 and will yield a family of control Hamiltonians $\hat{W}(t)$ also labeled by t_0 . This does not hold true in the non-Hermitian case: A dressing transformation that yields a physical $\hat{W}(t)$ for one value of t_0 might yield an unphysical $\hat{W}(t)$ for another value of t_0 .

III. EXAMPLE: TWO-MODE SYSTEM

To make things concrete, and without loss of generality, we consider a symmetrized two-mode non-Hermitian Hamiltonian

$$\hat{H}_{\text{sym}} = -\left(\Delta + i\frac{\Gamma}{2}\right)\hat{\sigma}_z + \Omega\hat{\sigma}_x, \quad (12)$$

that describes two coupled harmonic modes subject to damping [see Fig. 1 (a)]. Here, $\Delta = (\omega_1 - \omega_2)/2$, is the frequency detuning, Ω is the coupling strength, and $\Gamma = (\gamma_1 - \gamma_2)/2 > 0$ is the difference between the damping rates associated to the individual modes.

Equation (12) depends on three parameters, which using the language of the previous section, we label by the vector $\mathbf{p} = (\Delta, \Omega, \Gamma) \in \mathbb{R}^3$. In spite of its simplicity, Eq. (12) describes several state-of-the-art experimental platforms [29, 62, 67, 69, 72–74] where non-Hermitian STAs can be readily implemented.

A. Holomorphic change of frame operator

We start by showing how to find a holomorphic change of frame operator that diagonalizes Eq. (12). The spectrum of \hat{H}_{sym} is given by $\text{Sp}[\hat{H}_{\text{sym}}(\mathbf{p})] = \{\pm\sqrt{(\Delta + i\Gamma/2)^2 + \Omega^2}\}$ and has EP₂'s located in parameter space determined by the system of equations

$$\begin{aligned} -\frac{\Gamma^2}{4} + \Omega^2 + \Delta^2 &= 0, \\ \Delta\Gamma &= 0. \end{aligned} \quad (13)$$

The set of vectors $\mathbf{p}_{2,l} = (\Delta_l, \Omega_l, \Gamma_l)$, $l \geq 1$, obeying Eq. (13) form the parameter subspace B_2 where the spectrum is doubly degenerate. Since the spectrum of Eq. (12) only has EP₂'s, we have $B_{\text{deg}} = B_2$ and the subspace of parameters where the spectrum is non-degenerate is given by $B_{\text{ng}} = \mathbb{R}^3 \setminus B_2$.

Since the eigenvalues of \hat{H}_{sym} behave like the complex square root function, they are not holomorphic on all of B_{ng} . The region defined by

$$\begin{aligned} -\frac{\Gamma^2}{4} + \Omega^2 + \Delta^2 &\leq 0, \\ \Delta\Gamma &= 0, \end{aligned} \quad (14)$$

must be excluded as any \mathbf{p} belonging to this region is mapped to the interval $(-\infty, 0]$ which corresponds to the branch cut of the square root function [see Fig. 3(a)]. This shows the necessity of finding a different representation for the eigenvalues since any closed contour γ winding around B_2 necessarily intersects the branch cut region leading to a phase shift of the eigenvalues [see Fig. 3 (a)]. This prevents one from finding a change of frame operator that is holomorphic in B_{ng} .

To overcome this issue, we express the eigenvalues of Eq. (12) on the Riemann surface for the square root function [75] [see Fig. 3 (b)]. We have

$$\lambda_{\pm}(\mathbf{p}) = \pm\lambda(\mathbf{p}) = \pm \cos[\chi(\mathbf{p})] \sqrt{\left(\Delta + i\frac{\Gamma}{2}\right)^2 + \Omega^2}, \quad (15)$$

where χ is a function that geometrically accounts for the “gluing” of the two leaves of the square root function that make up the Riemann surface. Basically, the function χ is constructed to compensate for the π -phase shift incurred when crossing the branch cut such that there is a seamless transition from one leaf of the square root function to the other.

Using Eq. (15) we can find the right eigenmodes of \hat{H}_{sym} [see Eq. (2)] such that the coefficients of their decomposition are holomorphic functions as desired. We find

$$|\psi_j(\mathbf{p})\rangle = \left[-\left(\Delta + i\frac{\Gamma}{2}\right) + \lambda_j(\mathbf{p}) \right] |0\rangle + \Omega |1\rangle, \quad (16)$$

with $j \in \{+, -\}$. This immediately yields the change of frame operator that diagonalizes Eq. (12), and which is holomorphic on B_{ng} ,

$$\hat{S}_{\text{ad}}(\mathbf{p}) = \sum_{j=-,+} |\psi_j\rangle\langle\psi_j(\mathbf{p})|, \quad (17)$$

where $\langle\psi_j(\mathbf{p})|$ is a left eigenvector of \hat{H}_{sym} . Left eigenvectors obey the eigenvalue equation $\langle\psi_j|\hat{H}_{\text{sym}} = \lambda_j\langle\psi_j|$ and are related to the right eigenvectors by the orthogonality relation $\langle\psi_k|\psi_j\rangle = \delta_{k,j}$, where $\delta_{k,j}$ is the Kronecker delta function. In the frame that diagonalizes Eq. (12) the eigenvectors $|\psi_j\rangle$ are independent of \mathbf{p} (constant eigenvectors).

Finally, we note that for non-Hermitian Hamiltonians with special symmetry like Eq. (12), it is often possible to find the change of frame operator without having to explicitly find the eigenvalues and eigenvectors of \hat{H} . Here, by making the analogy to a spin-1/2 in an external magnetic field, the change of frame operator that diagonalizes the Hamiltonian can be found by aligning the quantization axis with the orientation of the spin (rotation of the coordinate system). We find that the holomorphic change of frame operator can also be written as

$$\hat{S}_{\text{ad}}(\mathbf{p}) = \exp\left[-\frac{i}{2}\theta(\mathbf{p})\hat{\sigma}_y\right], \quad (18)$$

with

$$\theta(\mathbf{p}) = -2 \arctan\left(\frac{\Omega}{\Delta + i\frac{\Gamma}{2} + \sqrt{(\Delta + i\frac{\Gamma}{2})^2 + \Omega^2}}\right) + \chi(\mathbf{p}). \quad (19)$$

We have defined the pseudo-rotation angle $\theta(\mathbf{p})$ using the half-angle identity $\arctan[y/x] = 2\arctan[y/(x +$

$\sqrt{x^2 + y^2})]$ to ensure χ is the same function as the one introduced in Eq. (15). In this case, χ “glues” together the leaves of the complex arctan function, which has a branch cut on the interval $(-i\infty, -i] \cup [i, i\infty)$, to ensure that $\theta(\mathbf{p})$ is holomorphic on $\mathbb{R}^3 \setminus B_{\text{ng}}$.

Performing the similarity transformation defined by Eq. (18) leads to

$$\hat{H}_{\text{diag}}(\mathbf{p}) = \hat{S}_{\text{ad}}^{-1}(\mathbf{p})\hat{H}_{\text{sym}}(\mathbf{p})\hat{S}_{\text{ad}}(\mathbf{p}) = \lambda(\mathbf{p})\hat{\sigma}_{z,\text{diag}}. \quad (20)$$

with $\lambda(\mathbf{p})$ given by Eq. (15), which immediately yields the holomorphic eigenvalues.

B. Topological operations with a two-mode system

We are now in a position to understand what kind of topological operations one can generate by winding around B_2 . To this end, we consider a closed, circular contour $\gamma_{\text{circ}}(\varepsilon)$ centered at $\mathbf{p}_{\text{center}} = (0, \Omega_0, \Gamma_0)$ with radius Δ_0 parameterized by

$$\begin{aligned} \Delta(\varepsilon) &= \Delta_0 \sin(\varepsilon + \varphi), \\ \Omega(\varepsilon) &= \Omega_0 + \Delta_0 \cos(\varepsilon + \varphi), \\ \Gamma(\varepsilon) &= \Gamma_0, \end{aligned} \quad (21)$$

with $\varepsilon \in [0, 1]$. The basepoint of $\gamma_{\text{circ}}(\varepsilon)$ can be unambiguously located in parameter space by specifying the center of the circle [see red dot in Fig. 3 (a)] and the angle φ [purple cross for $\varphi = 0$, orange cross for $\varphi = \pi$ in Fig. 3 (a)] with the Ω -axis in the $\Gamma = \text{const.}$ plane.

When $\gamma_{\text{circ}}(\varepsilon)$ is centered at $\mathbf{p}_{\text{center}}$, the function χ has the simple form

$$\chi(\varepsilon) = \pi\Theta\left[\frac{1-d}{2} + \left(\varepsilon - \frac{1}{2} + \frac{\varphi}{2\pi}\right)\right], \quad (22)$$

where $\Theta(x)$ is the Heaviside step function (with the convention $\Theta(0) = 1$) and the parameter d accounts for the loop orientation (± 1 for clockwise/counter-clockwise). For the rest of this article, and unless otherwise specified, we consider the closed contour $\gamma_{\text{circ}}(\varepsilon)$ centered at $\mathbf{p}_{\text{center}}$ with basepoint $\varphi = 0$ or $\varphi = \pi$.

Using Eqs. (15) and (22), we find that $\lambda_{\pm}[\mathbf{p}(\varepsilon)]$ trace a continuous eigenvalue braid that obeys

$$\lambda_{\pm}[\mathbf{p}(0)] \rightarrow -\lambda_{\pm}[\mathbf{p}(1)] = \lambda_{\mp}[\mathbf{p}(0)]. \quad (23)$$

While Eq. (23) is valid for any basepoint φ , the value of $\lambda_{\pm}[\mathbf{p}(0)]$ (end points of the braid) depends explicitly on the choice of basepoint φ (braids generated from loops with different basepoints are not isotopic since the isotopy of braids requires the end point to be fixed). We show this in Fig. 3 (c) where the braids traced for $\varphi = 0$ and $\varphi = \pi$ are compared.

The mapping of the initial to the final eigenvalues is described by the permutation $\sigma_1(\psi_{\pm}) = \psi_{\mp}$ [see Eq. (3)]. The corresponding topological operation is given by

$$\hat{P}_{\sigma_1} = |\psi_{+}[\mathbf{p}(0)]\rangle\langle\psi_{-}[\mathbf{p}(0)]| + |\psi_{-}[\mathbf{p}(0)]\rangle\langle\psi_{+}[\mathbf{p}(0)]|, \quad (24)$$

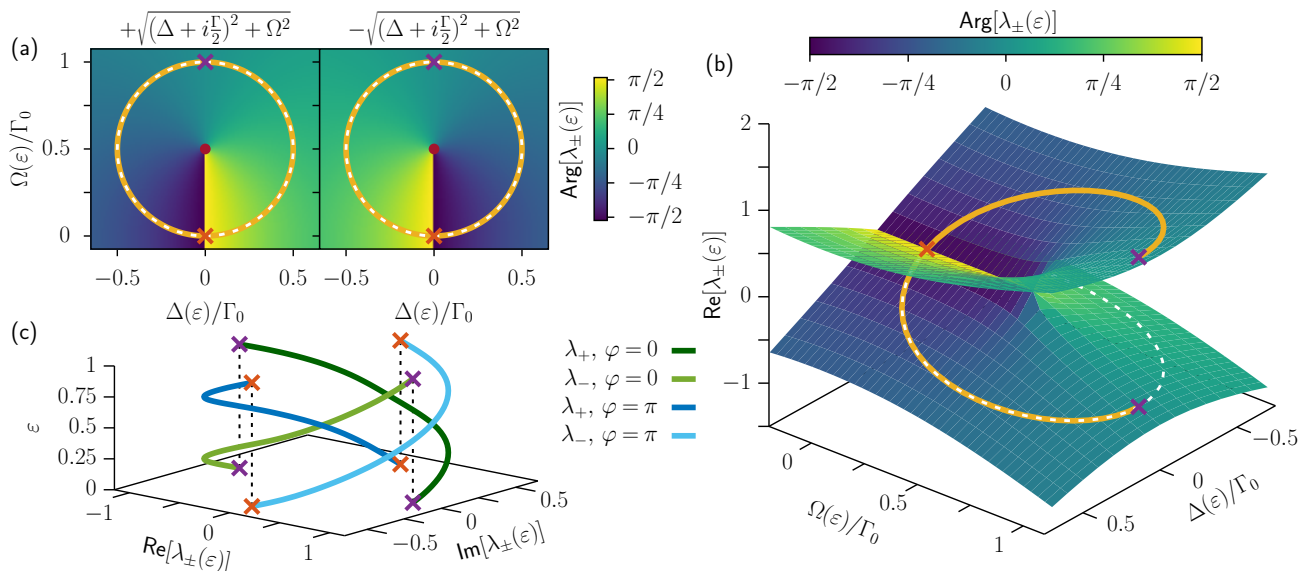


Figure 3. Riemann surface and topology of the square root function. (a) The argument of the eigenvalues of Eq. (12) in the vicinity of the EP (red dot). The yellow (white dashed) circle represents a circular contour $\gamma_{\text{circ}}(\varepsilon)$ with basepoint $\varphi = 0$ indicated by the purple cross ($\varphi = \pi$, orange cross) [see Eq. (21)]. The argument is discontinuous along the contour. (b) Defining the eigenvalues of the NH Hamiltonian on their associated Riemann manifold leads to holomorphic functions along $\gamma_{\text{circ}}(\varepsilon)$. Contours with different basepoints lead to different spectral flows [yellow and white dashed traces correspond to contours defined in (a)]. (c) Eigenvalues braiding associated to contours defined in (a).

which follows from Eq. (4). Since the mapping described by Eq. (23) is independent of the choice of contour (including the basepoint), $\sigma_n^\ell = \prod_{k=1}^\ell \sigma_n$ describes the eigenvalue permutation for any loop that winds ℓ times around B_2 .

The topological operation defined in Eq. (24) depends on the choice of basepoint φ , since the eigenmodes explicitly depend on φ [see Eqs. (16) and (21)]. This implies that $\hat{P}_{\sigma_1}(\varphi = 0) \neq \hat{P}_{\sigma_1}(\varphi = \pi)$.

C. Non-Hermitian Systems and Violation of the Adiabatic Theorem

The easiest way to implement the operation defined in Eq. (24) would be to adiabatically evolve \hat{H}_{sym} along $\gamma_{\text{circ}}(\varepsilon)$. As discussed in Sec. II B and extensively in the literature [22, 35, 62, 63], this is impossible for non-Hermitian systems. However, for completeness and to have a baseline to compare against non-Hermitian STAs, we briefly discuss below the dynamics generated by \hat{H}_{sym} when \mathbf{p} varies slowly in time.

To this end, we turn ε into a smooth, monotonic time-varying function defined by

$$\varepsilon(t) = d \left[6 \left(\frac{t}{t_0} \right)^5 - 15 \left(\frac{t}{t_0} \right)^4 + 10 \left(\frac{t}{t_0} \right)^3 \right], \quad (25)$$

which fulfills $\dot{\varepsilon}(0) = \dot{\varepsilon}(t_0) = \ddot{\varepsilon}(0) = \ddot{\varepsilon}(t_0) = 0$ (where $\ddot{x} = d^2x/dt^2$). This function varies from 0 to 1 for $t \in [0, t_0]$, with t_0 being the time needed to trace the loop $\gamma_{\text{circ}}(\varepsilon)$.

We refer to the time-generated loop as the control loop, and use the dimensionless quantity $\Gamma_0 t_0$ to refer to the loop time duration.

Expressing $\hat{H}_{\text{sym}}(t)$ [see Eq. (12)] in the frame of instantaneous eigenmodes via $\hat{S}_{\text{ad}}(t)$ [see Eqs. (6) and (18)], we obtain the adiabatic NH Hamiltonian

$$H_{\text{ad}}(t) = \lambda(t) \hat{\sigma}_{z,\text{ad}} - \frac{1}{2} \dot{\theta}(t) \hat{\sigma}_{y,\text{ad}}, \quad (26)$$

which we use to solve for the flow $\hat{\Phi}_{\text{ad}}(t)$ [see Eq. (5)]. Transition probabilities between instantaneous eigenmodes are then given by

$$P_{i,j}(t) = \frac{\left| \langle \psi_j | \hat{\Phi}_{\text{ad}}(t) | \psi_i \rangle \right|^2}{\sum_j \left| \langle \psi_j | \hat{\Phi}_{\text{ad}}(t) | \psi_i \rangle \right|^2}, \quad (27)$$

with $i, j \in \{+, -\}$.

We plot in Fig. 4 $P_{i,j}(t)$ as a function of $\Gamma_0 t$ for $\Delta_0 = \Omega_0 = \Gamma_0/2$, $\Gamma_0 t_0 = 50$, $\varphi = 0$, $d = 1$. When the system is initialized in the least damped mode ($|\psi_+\rangle$), we find as expected that $P_{+,+}(t) \simeq 1$ and $P_{+,-}(t) \simeq 0$ (blue and orange traces in Fig. 4(a), respectively) for all times. This indicates that $|\psi_+\rangle$ evolves adiabatically and $\lambda_+(t)$ traces the expected strand of the braid associated with $\gamma_{\text{circ}}(\varepsilon)$. However, when the system is initialized in the most damped mode ($|\psi_-\rangle$), we have $P_{-,-}(t) \neq 1$ and $P_{-,+}(t) \neq 0$ for all times (green and purple traces in Fig. 4(b), respectively), indicating that $|\psi_-\rangle$ is not evolving adiabatically; the small non-adiabatic transitions from $|\psi_-\rangle \rightarrow |\psi_+\rangle$ get exponentially enhanced due

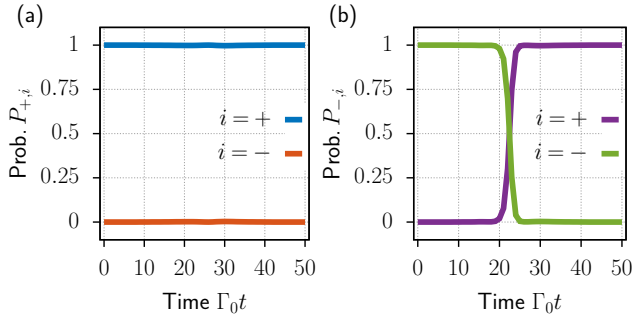


Figure 4. Non-reciprocal dynamics with a two-mode system. Implementing a clockwise control loop around an EP leads to (a) $P_{+,+}(t_0) = 1$ (blue trace), $P_{-,+} = 0$ (orange trace) and (b) $P_{-,+}(t_0) = 1$ (purple trace), $P_{-,-}(t_0) = 0$ (green trace).

to amplitude amplification of the least damped mode [31–33]. As a consequence, the strand of the braid associated to $\lambda_-(t)$ cannot be traced and the topological operation defined in Eq. (24) cannot be generated.

D. Near Ideal Permutation Operation via Near-Coherent Evolution

Among the (infinite) possibilities for a basepoint along $\gamma_{\text{circ}}(\varepsilon)$, there is a special choice corresponding to $\varphi = \pi$ that leads to $\text{Im}[\lambda_{\pm}(\mathbf{p}(\varepsilon))]$ being an anti-symmetric function with respect to $\varepsilon = 1/2$ [see Fig. 5(a)]. This leads to $\hat{\Phi}_{\text{ad}}(t_0)$ being “quasi” unitary for certain loop times $\Gamma_0 t_0$ since the imaginary part of the eigenvalues average out to zero during the evolution. We, thus, expect to observe interference phenomena akin of what has been observed in non-Hermitian PT-symmetric systems [53, 76–79].

We plot in Fig. 5(b) the non-adiabatic transition probabilities $P_{+,-}(t_0)$ (blue trace) and $P_{-,+}(t_0)$ (orange trace) evaluated at $t = t_0$ as a function of the loop time $\Gamma_0 t_0$. Our results show that for $\Gamma_0 t_0 > 1$ the non-adiabatic transition probability $P_{+,-}(t_0)$ almost vanishes. This necessarily implies that if the system is initialized in the least damped eigenmode ($|\psi_+\rangle$) at $t = 0$, it will end up in the same eigenmode at $t = t_0$. The situation is quite different when the system is initialized in the most damped mode ($|\psi_-\rangle$). For almost all values of $\Gamma_0 t_0$ the non-adiabatic transition probability is maximal $P_{-,+}(t_0) \simeq 1$, but there are special values of $\Gamma_0 t_0$ at which $P_{-,+}(t_0)$ vanishes. For those special times, the system ends up in the most damped eigenmode, if it is initially prepared in that eigenmode.

To verify our interpretation of the dynamics, we check that the flow $\hat{\Phi}_{\text{ad}}(t_0)$ is “quasi” unitary at the special values of $\Gamma_0 t_0$. In Fig. 5(c), we plot the spectral norm $\|\hat{\Phi}_{\text{ad}}^\dagger(t_0) - \hat{\Phi}_{\text{ad}}^{-1}(t_0)\|_2$ as a function of $\Gamma_0 t_0$. When the spectral norm is 0, we have $\hat{\Phi}_{\text{ad}}^\dagger(t_0) = \hat{\Phi}_{\text{ad}}^{-1}(t_0)$, which is the defining property of unitary operators.

In Fig. 5(d), we plot the transition probabilities

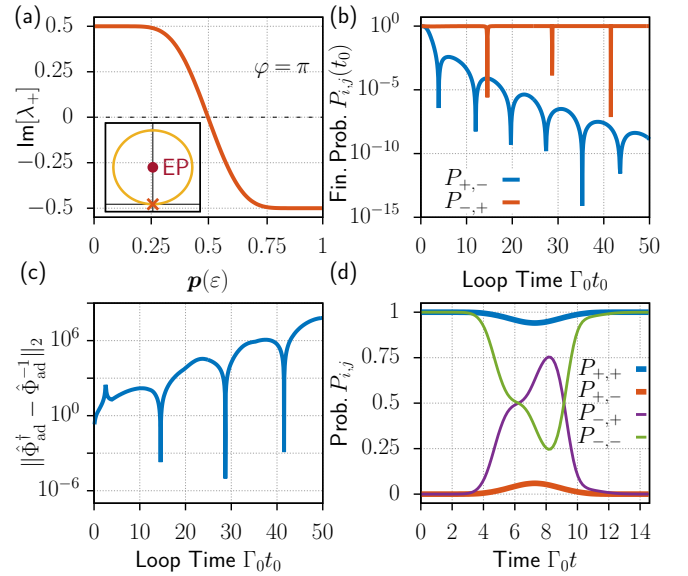


Figure 5. Dynamics with contours yielding near ideal topological operations. (a) Choosing $\varphi = \pi$ as a basepoint for $\gamma_{\text{circ}}(\varepsilon)$ yields a spectrum with an antisymmetric imaginary part that balances on average gain and loss. (b) Akin to coherent evolution there exists special loop times for which the final transition probabilities $P_{+,-}(t_0)$ and $P_{-,+}(t_0)$ vanish simultaneously. (c) For these special loop times, the flow associated with the NH Hamiltonian at $t = t_0$ is quasi-unitary, i.e., $\hat{\Phi}_{\text{ad}}^\dagger(t_0) \approx \hat{\Phi}_{\text{ad}}^{-1}(t_0)$. (d) Transition probabilities as a function of $\Gamma_0 t$ for the special loop time $\Gamma_0 t_0 = 14.5$.

$P_{+,+}(t)$ (thick blue trace), $P_{+,-}(t)$ (thick orange trace), $P_{-,+}(t)$ (thin purple trace), and $P_{-,-}(t)$ (thin green trace) as a function of $\Gamma_0 t$ for the special control loop time $\Gamma_0 t_0 = 14.5$. As one can observe the evolution of the eigenmodes is not adiabatic, but akin to a coherent evolution where destructive interference brings the system back to the desired eigenmode at $t = t_0$ after populating the other eigenmode at intermediate times. This also corresponds to the physical principle behind STAs, which only emulate adiabatic dynamics at the final time.

The difficulty in using these types of control loops to generate topological operation lies in achieving the exact timing at which $P_{-,+}(t_0)$ vanishes; any small deviations from these special loop times will result in $P_{-,+}(t_0) > 0$ [see orange trace Fig. 5(b)]. The idea of using a control loop that yields a spectrum with an anti-symmetric imaginary part with respect to $\varepsilon/2$ to emulate adiabatic dynamics has been previously reported [48, 49, 80].

E. Transitionless Driving

We are now ready to discuss the main results of this manuscript, the construction of non-Hermitian STAs. We start by deriving the non-Hermitian equivalent of the well-known STA coined Transitionless Driving (TD) [37, 39], which is designed to suppress non-adiabatic transi-

tions between the instantaneous eigenstates at all times. The dressing transformation [see Eq. (8)] leading to TD is the trivial dressing

$$\hat{S}_{\text{TD}}(t) = \mathbb{1}, \quad (28)$$

which guarantees that the dressed states $|\phi_j\rangle$ [see Eq. (8)] correspond at all times to the instantaneous eigenmodes $|\psi_j\rangle$ of \hat{H}_{sym} [see Eq. (7)].

Using Eq. (11), one readily finds the non-Hermitian control Hamiltonian associated to TD. In the frame of instantaneous eigenmodes of $\hat{H}_{\text{ad}}(t)$, we have

$$\hat{W}_{\text{ad,TD}}(t) = +i\hat{S}_{\text{ad}}^{-1}(t)\partial_t\hat{S}_{\text{ad}}(t) = \frac{1}{2}\dot{\theta}(t)\hat{\sigma}_{y,\text{ad}}, \quad (29)$$

where $\theta(t) = \theta\{\gamma_{\text{circ}}[\varepsilon(t)]\}$ with $\theta(\mathbf{p})$, $\gamma_{\text{circ}}(\varepsilon)$, and $\varepsilon(t)$ defined in Eqs. (19), (21), and (25), respectively. Like in the Hermitian case, $\hat{W}_{\text{ad,TD}}(t)$ is simply the opposite of the non-inertial term.

We stress once more the importance of constructing change of frame operators that are holomorphic to obtain the correct non-inertial term [see Sec. II C]. This includes the change of frame operator that diagonalizes the non-Hermitian Hamiltonian [see Eq. (12)] as well as the dressing transformation. If any of these are not holomorphic, it will lead to unphysical \hat{W} 's.

For the two-mode example considered here, this boils down to either defining the eigenvalues $\lambda(\mathbf{p})$ [see Eqs. (15) and (16)] or the pseudo-rotation angle $\theta(\mathbf{p})$ to be a holomorphic function of \mathbf{p} [see Eqs. (18) and (19)]. However, for this specific example, since we have $\dot{\chi}\{\gamma_{\text{circ}}[\varepsilon(t)]\} = 0$ [see Eqs. (19), (22), and (25)], using a non-holomorphic version of $\lambda(\mathbf{p})$ or $\theta(\mathbf{p})$ will also lead to the correct control operator [see Eq. (29)]. We discuss in Sec. III F 2 how failing to define the change of frame operator to be holomorphic generally leads to unphysical situations when considering higher-order STAs.

Like in the Hermitian case, the modified non-Hermitian Hamiltonian $\hat{H}_{\text{sym,TD}}(t) = \hat{H}_{\text{sym}}(t) + \hat{W}_{\text{sym,TD}}(t)$, with $\hat{W}_{\text{sym,TD}}(t) = \hat{S}_{\text{ad}}(t)\hat{W}_{\text{ad,TD}}(t)\hat{S}_{\text{ad}}^{-1}(t)$, emulates the expected ideal adiabatic dynamics. We compare in Fig. 6(a) [Fig. 6(b)] the transition probabilities $P_{+,+}(t)$ [$P_{-,-}(t)$] obtained with an uncorrected protocol (thick blue trace) against the TD protocol (orange trace). As expected with TD, we have $P_{+,+}(t) = P_{-,-}(t) = 1$ which indicates that the system remains at all times in the initial eigenmode.

We also compare in Figs. 6(c) and (d) the state-dependent fidelity error

$$\mathcal{E}_{i,i}(t_0) = 1 - P_{i,i}(t_0) \quad (30)$$

as a function of the control loop time $\Gamma_0 t_0$ for $i \in \{+, -\}$ between the uncorrected protocol (thick blue trace) and TD (orange trace). Our results show that TD behaves as in the Hermitian case, meaning one can view $\hat{W}_{\text{sym,TD}}(t)$ as a family of control operators labeled by the parameter t_0 . As we discuss below, and in contrast to the Hermitian case, this is in general not true for higher-order non-Hermitian STAs.

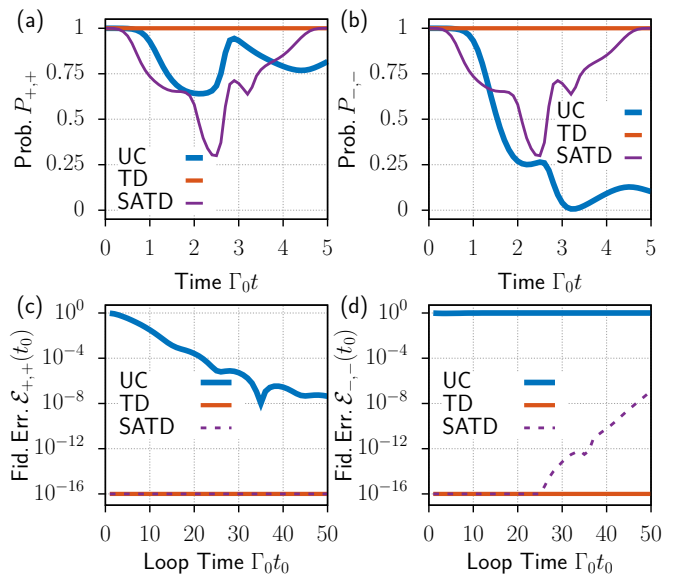


Figure 6. Comparison between uncorrected (UC, thick blue trace), TD (orange trace), and SATD (thin purple trace) control protocols. (a) Transition probability $P_{+,+}(t)$ and (b) $P_{-,-}(t)$ for $\Gamma_0 t_0 = 5$. (c) State dependent fidelity error $\mathcal{E}_{+,+}(t_0)$ and (d) $\mathcal{E}_{-,-}(t_0)$ as a function of $\Gamma_0 t_0$. TD traces the ideal braid at all times (see Sec. III E), while SATD guarantees that the end points of the generated braids coincide with those of the ideal case (see Sec. III F).

The numerical simulations were done using $\Delta_0 = \frac{1}{2}$, $\Omega_0 = \frac{1}{6}$, $\varphi = -\frac{\pi}{8}$, $d = 1$, and $\Gamma_0 t_0 = 5$ for Figs. 6(a) and (b), and $\Delta_0 = \Omega_0 = \Gamma_0/2$, $\varphi = 0$, and $d = 1$ for Figs. 6(c) and (d).

1. Transitionless driving dynamics

For the Hermitian case, the TD correction modifies the *coherent* dynamics of the system such that when the system is initialized in one of the old eigenmodes [an eigenmode of $\hat{H}_{\text{sym}}(t)$ as opposed to an eigenmode of $\hat{H}_{\text{sym,TD}}(t)$], destructive interference prevents transitions at all times to the other old eigenmode.

For non-Hermitian systems, this interpretation cannot hold since we are dealing with dissipative dynamics. The generalization would be that the non-Hermitian version of TD modifies the *incoherent* dynamics such that the effective decay rate of an old eigenmode corresponds to the “ideal” decay rate associated to the adiabatic approximation of $\hat{H}_{\text{sym}}(t)$. This implies, like in the Hermitian case, that $\hat{H}_{\text{sym,TD}}(t)$ generates a dynamics that mimics the idealized adiabatic dynamics of \hat{H}_{sym} . There is, however, another possible explanation for what the non-Hermitian TD correction does. It modifies the control loops such that they wind around an exceptional point of the modified spectrum [the spectrum of $\hat{H}_{\text{sym,TD}}(t)$] in such a way that the generated dynamics happens to be close to the ideal adiabatic dynamics of $\hat{H}_{\text{sym}}(t)$ (similar

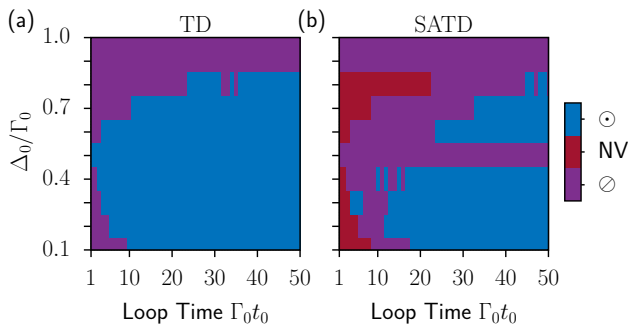


Figure 7. STAs validity. Exceptional point encircling check [see Eq. (A1)] for (a) TD correction [see Sec. III E] and (b) SATD correction [see Sec. III F]. We find that TD and SATD ensure eigenvalue braiding for all (applicable) parameter sets, but the EP associated to $\hat{H}_{\text{sym,STA}}$ is not necessarily encircled. The labeling scheme is as follows: \odot - EP encircled, \oslash - EP not encircled, NV - not a valid STA. Braiding of the eigenvalues associated to $\hat{H}_{\text{sym,mod}}$ is observed for all (applicable) parameter sets.

to having control loops that lead to the imaginary part of the spectrum to be anti-symmetric, see Sec. III D).

To distinguish between these two scenarios, we checked if the modified control loops wind around an EP associated to $\hat{H}_{\text{sym,TD}}(t)$ (see Appendix A).

We plot in Fig. 7(a) as a function of loop time $\Gamma_0 t_0$ and radius Δ_0/Γ_0 [see Eq. (21)] a map showing when the TD modified control loop winds around an EP associated to the spectrum of $\hat{H}_{\text{sym,TD}}(t)$ (blue) or does not (purple). We check this for $1 \leq \Gamma_0 t_0 \leq 50, 0.1 \leq \Delta_0 t_0 \leq 1, \varphi = 0, \Omega_0 = \Gamma_0/2$, and $d = 1$. Our result show that the modified control loop does not necessarily wind around an EP of the modified spectrum, but as discussed earlier, the dynamics always yields an eigenvalue braid. This indicates that the non-Hermitian version of TD, similar to the Hermitian case, emulates the ideal adiabatic dynamics.

2. Choice of initial control loop

In Sec. III D we showed that a different choice of basepoint along the same closed contour can result in control loops that generate a dynamics yielding the desired topological operation [see Eq. (24)] without tracing the ideal eigenvalue braid. Since this particular choice of control loop can lead to the desired dynamics without applying a correction, one might presume that it will lead to a more energy-effective TD correction since there is “less” to correct.

We plot in Fig. 8(a) the root mean square (RMS) amplitude of the fields used to implement a specific dynamics as a function of control loop time $\Gamma_0 t_0$. Since the control fields can be complex, we define the RMS ampli-

tude to be

$$\text{RMS} = \sqrt{\frac{1}{t_0} \int_0^{t_0} dt \sum_{i=x,y,z} |f_i(t)|^2}. \quad (31)$$

where $f_i(t)$ is the coefficient of the decomposition of $\hat{H}(t)$ associated to the Pauli operator $hat{\sigma}_i$ with $i \in \{x, y, z\}$. We show this for the uncorrected fields (UC) associated to the initial control loop [see Eq. (21)], and the TD correction $\hat{W}_{\text{sym,TD}}$ for $\varphi = 0$ and $\varphi = \pi$. We used $\Delta_0 = \Omega_0 = \Gamma_0/2$, and $d = 1$.

Our results indicate that there is no significant energy reduction in implementing TD when choosing an initial control loop with basepoint $\varphi = \pi$; more precisely for $\Gamma_0 t_0 \gtrsim 5$ the RMS field amplitude of $\hat{H}_{\text{sym}}(t)$ (solid traces) and $\hat{H}_{\text{sym,TD}}(t)$ (dashed traces) is nearly the same for both $\varphi = 0$ (solid blue and dashed orange traces) and $\varphi = \pi$ (solid purple and dashed green traces).

We further check that there is no significant difference in the control field amplitudes for the special loop times that generate “STA-like” dynamics when $\varphi = \pi$ [see Fig. 5]. We show this behavior in Figs. 8(b) and 8(c) where we plot the real and imaginary parts, respectively, of the matrix elements of $\hat{W}_{\text{sym,TD}}$ for $\varphi = 0$ (orange trace) and $\varphi = \pi$ (green trace) for $\Gamma_0 t_0 \approx 14.5$.

This is to be expected since the TD correction is designed to cancel non-adiabatic transitions between the eigenmodes of \hat{H}_{sym} at all times. From a resource-cost point of view, TD can therefore not benefit from the dynamics happening at special values of $\Gamma_0 t_0$ and $\varphi = \pi$, since there are still non-adiabatic transitions that need to be canceled at intermediate times.

F. Super Adiabatic Transitionless Driving

Despite its effectiveness, the TD correction may be considered too demanding, as it often requires considerable resources to be implemented [81], e.g., for the two-mode model considered here one must be able to couple to $\hat{\sigma}_y$ and tune the interaction. To overcome this limitation, an STA coined superadiabatic transitionless driving (SATD) was introduced [38, 43]. SATD is known to yield correction fields that are compatible with the constraints of a two-level system and a lambda system [43, 44].

Fundamentally, SATD is a special case of the dressed state approach to STAs in which the dressing is chosen to diagonalize the adiabatic Hamiltonian (which includes the non-inertial term that couples the instantaneous eigenmodes [see Eq. (26)]).

For Hermitian systems, independently of the protocol time t_0 , SATD allows one to engineer a modified Hamiltonian $\hat{H}_{\text{sym,SATD}}(t)$ that evolves a set of chosen eigenstates $|\psi_i(t)\rangle$ of $\hat{H}(t)$ such that $|\psi_i(0)\rangle$ is mapped to $|\psi_i(t_0)\rangle$ without enforcing the system to occupy $|\psi_i(t)\rangle$ at all intermediate times. For non-Hermitian systems, as we discuss below, SATD does not yield for all values

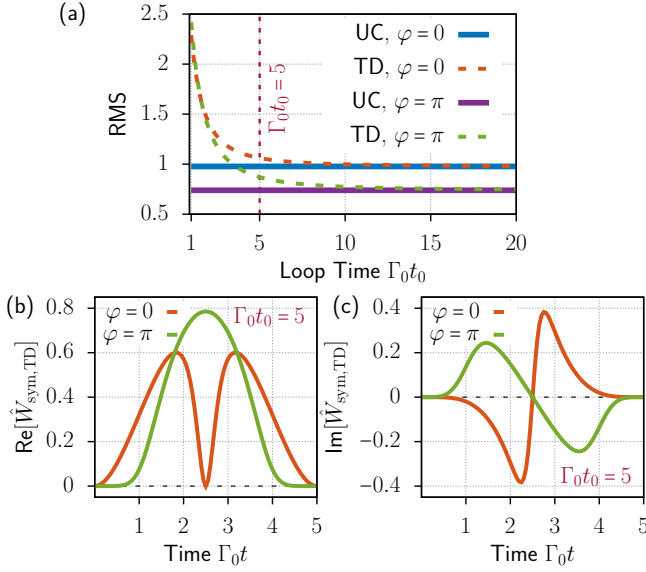


Figure 8. RMS amplitude for TD correction. (a) Comparison of RMS [see Eq. (31)] amplitudes between uncorrected case (UC, solid lines) and TD (dashed lines) for $\varphi = 0$ (blue and orange traces) and $\varphi = \pi$ (purple and green). Example of (b) real and (c) imaginary parts of the TD correction \hat{W}_{TD} for $\Gamma_0 t_0 = 14.5$. Leveraging the quasi-coherent regime of the uncorrected dynamics does yield TD fields with reduced energy (see main text for more details).

of t_0 a modified Hamiltonian that generates the desired mapping. The SATD solutions cannot, therefore, be considered as a family of solutions labeled by the protocol time t_0 .

1. SATD Dressing Transformation

For the two-mode system described by Eq. (12), the SATD dressing operator, which coincides with the change of frame operator that diagonalizes $\hat{H}_{\text{ad}}(t)$, is given by

$$\hat{S}_{\text{SATD}}(t) = \exp\left[-\frac{i}{2}\mu(t)\hat{\sigma}_x\right], \quad (32)$$

where the holomorphic dressing angle is

$$\begin{aligned} \mu(t) &= \mu_{\text{nat}}(t) + \chi_{\mu}(t) \\ &= -\arctan\left[\frac{1}{2}\frac{\dot{\theta}(t)}{\lambda(t)}\right] + \chi_{\mu}(t). \end{aligned} \quad (33)$$

Here, $\lambda(t)$ and $\theta(t)$ are given by Eqs. (15) and (19), respectively, and the time dependence is acquired through a choice of control loop $\gamma[\varepsilon(t)]$, i.e., $\mu(t) = \mu\{\gamma[\varepsilon(t)]\}$. The function $\chi_{\mu}(t)$ is defined by

$$\chi_{\mu}(t) = \pi \sum_s \Theta(t - t_s), \quad (34)$$

with $\Theta(x)$ defined below Eq. (22) and t_s corresponds to the times at which the control loop “crosses” the branch cut associated to $\mu_{\text{nat}}(t)$. Geometrically, one can view $\chi_{\mu}(t)$ as a function that glues together the leaves of $\mu_{\text{nat}}(t)$ to make up the Riemann surface, on which $\mu(t)$ is holomorphic.

Constructing the holomorphic dressing angle from the natural dressing angle does not necessarily guarantee that the boundary properties are conserved. Equation (33) shows that even if one has initially engineered a control loop that fulfills $\mu_{\text{nat}}(0) = \mu_{\text{nat}}(t_0) = 0$, we have $\mu(t_0) = n\pi$, where n is the number of times the branch cut associated to $\mu(t)$ is crossed. Thus, $\hat{S}_{\text{SATD}}(t_0)$ is not necessarily the identity transformation as required (see Sec. II C) since

$$\hat{S}_{\text{SATD}}(t_0) = \exp\left[-\frac{i}{2}(n\pi)\hat{\sigma}_x\right] = (-i)^n \hat{\sigma}_x^n. \quad (35)$$

If n is an even integer then Eq. (35) reduces to $(i)^n \mathbb{1}$ and Eq. (9) is fulfilled up to an (irrelevant) global phase. However, if n is an odd integer, then Eq. (35) reduces to $(i)^n \hat{\sigma}_x$, which violates Eq. (9) and immediately shows that in this case one cannot obtain a valid STA.

For a choice of control loop $\gamma[\varepsilon(t)]$, there are several parameters that can control how many times the branch cut associated to $\mu_{\text{nat}}(t)$, including the loop time $\Gamma_0 t_0$. Thus, and in stark contrast to the Hermitian case, the non-Hermitian version of SATD cannot be seen as a family of solutions labeled by the control loop time $\Gamma_0 t_0$. We illustrate this behavior in Fig. 9(a) where we plot the value of $\mu(t_0)/\pi \text{Mod} 2$ as a function of $\Gamma_0 t_0$ for two different circular contours $\gamma_{\text{circ},1}[\varepsilon(t)]$ (blue trace) and $\gamma_{\text{circ},2}[\varepsilon(t)]$ (orange trace) [see Eq. (25)].

We choose $\Delta_0 = \Omega_0 = \Gamma_0/2, \varphi = 0, d = 1$ for $\gamma_{\text{circ},1}$, and $\Delta_0 = \Gamma_0/2, \Omega_0 = \Gamma_0/6, \varphi = -\pi/8, d = 1$ for $\gamma_{\text{circ},2}$. The dressing angle obtained from $\gamma_{\text{circ},1}[\varepsilon(t)]$ always yields a valid SATD protocol, i.e., the dressing transformation obeys conditions (1)-(3) of the dressed state approach to non-Hermitian STAs (see Sec. II C), while the dressing angle obtained from $\gamma_{\text{circ},2}[\varepsilon(t)]$ only leads to a valid SATD protocol for certain values of $\Gamma_0 t_0$.

We plot in Figs. 9(b) and (c) the real and imaginary parts of $\mu_{\text{nat}}(t)$ (dashed orange trace) and $\mu(t)$ (solid blue trace) [see Eq. (33)] obtained with $\gamma_{\text{circ},2}[\varepsilon(t)]$ as a function of time for $\Gamma_0 t_0 = 2$ [corresponding to the green dashed line in Fig. 9(a)]. Turning the natural dressing angle into its holomorphic counterpart leads to a dressing angle that does not vanish at $t = t_0$ and, thus, cannot be used to define a valid SATD dressing transformation. In contrast, for $\Gamma_0 t_0 = 5$ [corresponding to the purple dashed line in Fig. 9(a)], one obtains a holomorphic dressing angle that vanishes at the end points and leads to a valid SATD protocol. This is illustrated in Fig. 9(d) where we plot both the real parts of $\mu_{\text{nat}}(t)$ (dashed orange trace) and $\mu(t)$ (blue solid trace).

We stress that this behavior is generic for any finite dimension and dressing choice, and is neither specific to the two-mode model we consider nor the SATD dressing.

2. Non-Hermitian SATD Control Hamiltonian

In the dressed frame defined by the SATD transformation [see Eq. (32)], the non-Hermitian SATD control Hamiltonian is given by

$$\hat{W}_{\text{dr,SATD}}(t) = i\hat{S}_{\text{SATD}}^{-1}(t)\partial_t\hat{S}_{\text{SATD}}(t) = \frac{1}{2}\dot{\mu}(t)\hat{\sigma}_x, \quad (36)$$

and is only defined when $\hat{S}_{\text{SATD}}(0) = \hat{S}_{\text{SATD}}(t_0) = \mathbb{1}$ [see Eq. (9)] up to a global phase. Transforming Eq. (36) to the original lab frame yields

$$\begin{aligned} \hat{W}_{\text{sym,SATD}}(t) &= \hat{S}_{\text{ad}}\hat{S}_{\text{SATD}}\hat{W}_{\text{dr,SATD}}\hat{S}_{\text{SATD}}^{-1}\hat{S}_{\text{ad}}^{-1} \\ &= g_x(t)\hat{\sigma}_x + g_z(t)\hat{\sigma}_z, \end{aligned} \quad (37)$$

where we omitted the explicit time dependence of the change of frame operators in the first line for simplicity. The control fields are given by

$$\begin{aligned} g_x(t) &= -\Omega(t) + \frac{\dot{\theta}(t)}{2} \cot \mu(t) \sin \theta(t) + \frac{\dot{\mu}(t)}{2} \cos \theta(t) \\ g_z(t) &= \frac{i\Gamma}{2} + \Delta(t) + \frac{\dot{\theta}(t)}{2} \cot \mu(t) \cos \theta(t) - \frac{\dot{\mu}(t)}{2} \sin \theta(t). \end{aligned} \quad (38)$$

In Sec. III E 1, we stressed that for the two-mode case there was no difference in using $\hat{S}_{\text{ad}}(t)$ [see Eq. (18)] or a non-holomorphic version of it to obtain $\hat{W}_{\text{ad,TD}}(t)$ [see Eq. (29)]. However, Eq. (37) shows that using the non-holomorphic version of $\hat{S}_{\text{ad}}(t)$ leads to an invalid STA. The π -phase jumps (see Sec. III A) will result either in $g_x(t)$ and $g_z(t)$ being discontinuous or having the wrong sign.

3. SATD Dynamics

As for the Hermitian case, the SATD modified non-Hermitian Hamiltonian $\hat{H}_{\text{sym,SATD}}(t) = \hat{H}_{\text{sym}}(t) + \hat{W}_{\text{sym,SATD}}(t)$ generates a dynamics that maps an eigenmode $|\psi_i(0)\rangle$ of $\hat{H}_{\text{sym}}(t)$ prepared at $t = 0$ to $|\psi_i(t_0)\rangle$ without occupying $|\psi_i(t)\rangle$ at all times. We show this in Figs. 6(a) and 6(b) where we plot the transition probability $P_{i,i}(t)$ (thin solid purple trace) as a function of time for $\Gamma_0 t_0 = 5$ for $i \in \{+, -\}$. The transition probability obeys $P_{i,i}(0) = P_{i,i}(t_0) = 1$ while $P_{i,i}(t) \neq 1$ as expected. The numerics were performed with the same control loop as the one used in Sec. III E 1.

We also show in Figs. 6(c) and (d) the behavior of the state dependent fidelity errors $\mathcal{E}_{i,i}(t_0)$ as a function of $\Gamma_0 t_0$ [see Eq. (30)] for $i \in \{+, -\}$, respectively. Our results show that for a valid SATD protocol (see Sec. III F 1) we can always map $|\psi_i(0)\rangle$ to $|\psi_i(t_0)\rangle$. This implies that although the dynamics generated by $\hat{H}_{\text{sym,SATD}}$ does trace the ideal eigenvalue braids associated to $\hat{H}_{\text{sym}}[\gamma(\varepsilon)]$, it still allows one to generate the topological permutation operation defined in Eq. (24).

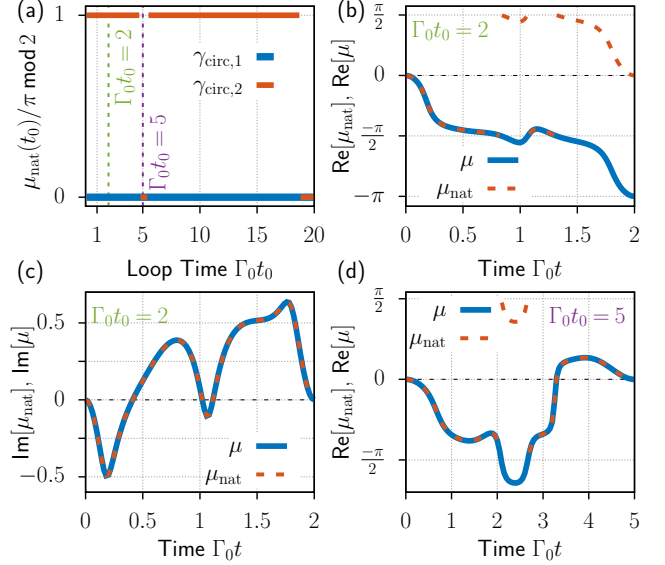


Figure 9. Determining the validity of SATD. (a) SATD is not a valid STA over the whole range $\Gamma_0 t_0 = [0, 25]$ for $\gamma_{\text{circ},2}$ (see main text for details) while it is a valid STA for $\gamma_{\text{circ},1}$ over the same range $\Gamma_0 t_0$. Real (b) and imaginary (c) parts of $\mu(t)$ and $\mu_{\text{nat}}(t)$ [see Eq. (33)] obtained with $\gamma_{\text{circ},2}$ leading to an invalid STA ($\Gamma_0 t_0 = 2$). (d) Same as (b) but using $\gamma_{\text{circ},1}$, which leads to a valid STA ($\Gamma_0 t_0 = 5$).

Similar to our analysis of the TD correction in Sec. III E, we check if the non-trivial braids traced by $\hat{H}_{\text{sym,SATD}}(t)$ are linked to encircling an EP associated to the modified spectrum. Our results are displayed in Fig. 7(b) where we show as a function of loop time $\Gamma_0 t_0$ and radius Δ_0/Γ_0 a map indicating if an EP of $\hat{H}_{\text{sym,SATD}}(t)$ is encircled or not when a non-trivial braid is traced. We check this using $1 \leq \Gamma_0 t_0 \leq 50, 0.1 \leq \Delta_0 t_0 \leq 1, \varphi = 0, \Omega_0 = \Gamma_0/2$, and $d = 1$. Similarly to TD (see Sec. III E), we conclude that a valid SATD protocol always leads to a non-trivial braid regardless of winding around an EP associated to $\hat{H}_{\text{sym,SATD}}(t)$.

4. Choice of Initial Control Loop

In Sec. III D, we discussed that there exists choices of base points for the same contour that can lead to the imaginary part of the spectrum to be anti-symmetric with respect to $t = t_0/2$. Evolving the system along the associated control loop and fine-tuning the duration of the loop leads to $P_{i,i}(t_0) = 1$ for $i \in \{+, -\}$ [see Fig. 5], but with $P_{i,i}(t) \neq 1$ for intermediate times.

In Fig. 10(a) we compare the RMS amplitude [see Eq. (31)] of the fields needed to implement the initial (uncorrected, UC) circular control loop (solid traces) [see Eq. (21)] and the associated SATD protocol (dashed traces) as a function of loop time $\Gamma_0 t_0$ for both $\varphi = 0$ (blue and orange traces) and $\varphi = \pi$ (purple and green traces), with the latter choice yielding a spectrum with

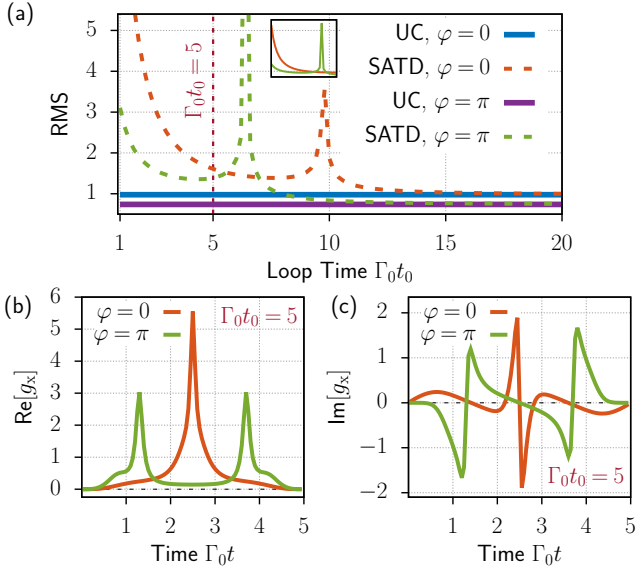


Figure 10. RMS amplitude for SATD correction. (a) Comparison of RMS [see Eq. (31)] amplitudes between uncorrected case (UC, solid lines) and SATD (dashed lines) for $\varphi = 0$ (blue and orange traces) and $\varphi = \pi$ (purple and green). Example of (b) real and (c) imaginary parts of $g_x(t)$ [see Eq. (38)] for $\Gamma_0 t_0 = 5$. There is no appreciable difference for the $g_z(t)$ control field. Choosing $\varphi = \pi$ yields control fields with an overall reduced amplitude.

an anti-symmetric imaginary part with respect to $t_0/2$. In our numerics, we further use $\Delta_0 = \Omega_0 = \Gamma_0/2$, $\varphi = 0$, and $d = 1$.

Deriving the SATD correction from a control loop with basepoint $\varphi = \pi$ yields on average a modified protocol that requires less resources to be implemented. In particular, choosing $\varphi = \pi$ and tuning the loop time $\Gamma_0 t_0$ to yield quasi-unitary dynamics [see Figs. 5(b) and (c)] leads to SATD control fields that have an amplitude which is more than 50% smaller than those obtain with $\varphi = 0$. We illustrate this behavior in Figs. 10(b) and (c) where we plot the real and imaginary parts of $g_x(t)$ [see Eq. (38)] for $\Gamma_0 t_0 = 14.5$, respectively. The orange (green) traces in Figs. 10(b) and (c) correspond to choosing $\varphi = 0$ ($\varphi = \pi$).

In contrast to TD (see Sec. III E 2), the resources needed to implement SATD can largely be reduced by choosing an initial control loop that yields a quasi-unitary dynamics that almost perfectly maps $|\psi_i(0)\rangle$ to $|\psi_i(t_0)\rangle$. This simply follows from the SATD philosophy, which does not enforce the ideal adiabatic dynamics at all times, but only at the initial and final times. Thus, for those special control loops, SATD needs to correct the dynamics “less”, which translates into correction fields with smaller amplitudes.

G. Robustness Analysis

For Hermitian systems, STAs inherit some of the robustness against parameter uncertainties from the adiabatic protocol they originate from [40, 45, 47, 81, 82]. Since parameter uncertainties are a form of quasi-static noise, they induce small-amplitude, noise-mediated transitions that are suppressed due to a large energy gap between instantaneous eigenmodes. To a certain degree, this behavior is an extension of the adiabatic theorem for small-amplitude, noise-mediated transitions between eigenmodes.

For non-Hermitian systems, however, since the adiabatic theorem does not hold (see Sec. II B), one might conclude that STAs offer no intrinsic form of robustness against parameter uncertainties. While this is true in the long loop-time limit ($\Gamma_0 t_0 \gg 1$), where any small amplitude transitions from the most- to the least-lossy mode are exponentially amplified (see Sec. III C), it is not the case in the short loop-time limit ($\Gamma_0 t_0 \lesssim 1$) since noise-mediated transitions are only marginally amplified.

To understand how parameter uncertainties give rise to noise-mediated transitions, it is enough to consider the scenario where there is an uncertainty in the amplitude of the control fields of \hat{H}_{sym} [see Eq. 12] generating the control loop $\gamma_{\text{circ}}\{\mathbf{p}[\varepsilon(t)]\}$. Specifically, we take the parameter Δ_0 [see Eq. (21)] to incur an uncertainty of $\delta\Delta_0$. Here, without loss of generality, we assume that $\delta\Delta_0$ is characterized by a normal Gaussian distribution

$$p(\delta\Delta_0) = \frac{1}{\beta\sqrt{2\pi}} \exp\left[-\frac{1}{2}\left(\frac{\delta\Delta_0}{\beta}\right)^2\right], \quad (39)$$

with mean $\langle\delta\Delta_0\rangle_{\delta\Delta_0} = 0$ and variance $\langle\delta\Delta_0^2\rangle_{\delta\Delta_0} = \beta^2$, where $\langle\cdot\rangle_{\delta\Delta_0}$ denotes averaging over the stochastic variable $\delta\Delta_0$.

Within this framework, the non-Hermitian Hamiltonian describing the evolution of the system is $\hat{H}_{\text{sym,imp}}(t) = \hat{H}_{\text{sym}}(t) + \delta\Delta_0\hat{\sigma}_z$, which in the adiabatic frame of $\hat{H}_{\text{sym}}(t)$ takes the form

$$\begin{aligned} \hat{H}_{\text{ad,imp}}(t) &= \hat{S}_{\text{ad}}^{-1}(t)\hat{H}_{\text{sym,imp}}(t)\hat{S}_{\text{ad}}(t) - i\hat{S}_{\text{ad}}^{-1}(t)\partial_t\hat{S}_{\text{ad}}(t) \\ &= \hat{H}_{\text{ad}}(t) + \delta\Delta_0(\cos[2\theta(t)]\hat{\sigma}_z - \sin[2\theta(t)]\hat{\sigma}_x), \end{aligned} \quad (40)$$

with $\hat{H}_{\text{ad}}(t)$ given in Eq. (26). Equation (40) shows that any uncertainty on the parameter Δ_0 will result in non-adiabatic-like transitions which cannot be corrected with STAs since the value of $\delta\Delta_0$ is unknown.

To illustrate the robustness of STAs in the short-time limit, we plot in Fig. 11 the noise-averaged average fidelity error

$$\begin{aligned} \langle\mathcal{E}_{i,j}(t)\rangle_{\delta\Delta_0} &= 1 - \langle P_{i,j}(t)\rangle_{\delta\Delta_0} \\ &= 1 - \int_{-\infty}^{\infty} d\delta\Delta_0 p(\delta\Delta_0) \frac{|\langle\psi_j|\hat{\Phi}_{\text{ad,imp}}(t)|\psi_i\rangle|^2}{\sum_j |\langle\psi_j|\hat{\Phi}_{\text{ad,imp}}(t)|\psi_i\rangle|^2}, \end{aligned} \quad (41)$$

as a function of the loop time $\Gamma_0 t_0$ for the uncorrected circular control loop [see Eq. (21)] (UC, blue trace) and the

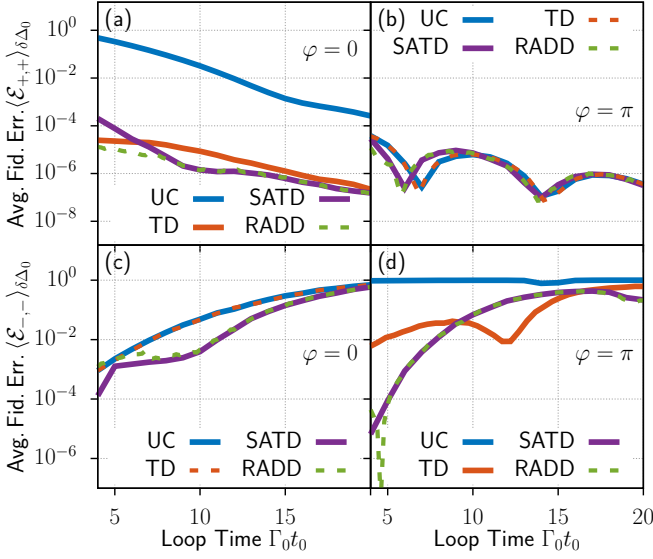


Figure 11. Robustness of STAs against parameter uncertainties. (a) Average state fidelity error $\langle \mathcal{E}_{+,+}(t_0) \rangle$ [see Eqs. (30) and Eq. (41)] as a function of $\Gamma_0 t_0$ for the circular control loop γ_{circ} [see Eq. (25)] using $\varphi = 0$. (b) Same as (a) but with $\varphi = \pi$ [see Fig. 5 and Sec. III D]. (c) Same as (a) for $\langle \mathcal{E}_{-,-}(t_0) \rangle$. (d) Same as (c) for $\varphi = \pi$.

associated TD (orange trace) and SATD (purple trace) protocols for both $\varphi = 0$ (see Figs. 11(a) for $i = j = +$ and (c) for $i = j = -$) and $\varphi = \pi$ (see Figs. 11(b) for $i = j = +$ and (d) for $i = j = -$). The numerics were performed by choosing $4 \leq \Gamma_0 t_0 \leq 50$, $\Delta_0 = \Omega_0 = \Gamma_0/2$, $\varphi = 0$, and $d = 1$.

Our results show the anticipated behavior: Non-Hermitian STAs provide a certain degree of robustness against parameter uncertainties in the short loop-time limit and allow one to generate the desired topological operation with high-fidelity for loop times fulfilling the condition $\Gamma_0 t_0 \lesssim 7$.

In principle, the non-Hermitian versions of TD and SATD should allow one to realize eigenvalue braiding in an experimental setup, even in the presence of uncertainties, given that one performs a “fast” control loop. However, this requires one to realize control fields with relatively large amplitudes since the corrections fields scale like $1/t_0$ [see Eq. (29) for TD, and Eq. (36) for SATD].

In the next section, we show how an appropriate choice of dressing leads to control fields with a moderate amplitude even in the short loop-time limit. This type of STA can be much easier to implement for a given experimental platform.

1. Reduced Amplitude Dressed Driving

We design a dressing that yields control fields with an RMS amplitude [see Eq. (31)] smaller than TD and SATD in the short loop-time limit. To this end, we con-

sider a modification of the SATD dressing angle given by

$$\mu_{\text{mod}}(t) = -\arctan \left[\frac{\frac{1}{2}\dot{\theta}(t)}{\lambda(t)[1 + F(t)]} \right], \quad (42)$$

where

$$F(t) = A \exp \left[-\left(\frac{t - t_0/2}{\nu} \right)^{2n} \right], \quad (43)$$

is a hyper-Gaussian mask function with free parameters A , ν , and n . The purpose of $F(t)$ is to reduce the overall amplitude of the control fields $g_x(t)$ and $g_z(t)$ [see Eq. (38)] by substituting $\mu(t) \rightarrow \mu_{\text{mod}}(t)$ since the fields are proportional to the amplitude of $\mu(t)$ and its first derivative. This defines a new STA which we coin Reduced Amplitude Dressed Driving (RADD).

To minimize the amplitude of $g_x(t)$ and $g_z(t)$ we look for the set of values $\{A, \nu, n\}$ that minimize the RMS amplitude [see Eq. (31)] of the control fields for a given t_0 . The minimization procedure is done by considering finite ranges for A , n , and ν . We chose $A \in [10^{-2}, 10]$, $n \in [1, 7]$, and $\nu \in [t_0/25, t_0/3]$.

In Fig. 12(a), we plot the RMS amplitude as a function of loop time $\Gamma_0 t_0$ for the uncorrected fields of $\hat{H}_{\text{sym}}(t)$ (UC, blue trace) [see Eq. (12)] and the associated TD (dashed orange trace), SATD (solid purple trace), and RADD (dashed green trace) STAs. The numerics were performed with $1 \leq \Gamma_0 t_0 \leq 20$, $\Delta_0 = \Omega_0 = \Gamma_0/2$, and $d = 1$.

As our results show, there is a range of control loop times $\Gamma_0 t_0 \gtrsim 10$ for which the control fields associated to the RADD dressing have an RMS amplitude smaller than those of TD and SATD. For $\Gamma_0 t_0 = 7$, the upper-bound limit of loop times we found that yields robust STAs in spite of parameter imprecisions [see Fig. 11], the RADD RMS value is similar to TD and UC, and 25% smaller than SATD. Similarly to SATD, RADD allows one to trace an eigenvalue braid that is not necessarily equivalent to the eigenvalue braid defined by \hat{H}_{sym} , but still fulfills Eqs. (23), thus, generating the desired topological operation [see Eq. (24)].

We can further reduce the RMS amplitude of the control fields by choosing the base point of the control loop such that $\text{Im}[\lambda_{\pm}(t)]$ is anti-symmetric with respect to $t = t_0/2$, i.e., setting $\varphi = \pi$ and $\Omega_0 = \Gamma_0/2$ [see Fig. 5 and Sec. III D]. We compare in Fig. 12(b) the RMS amplitudes of the fields when $\varphi = \pi$. At $\Gamma_0 t_0 = 7$, the RADD RMS (dashed green line) is similar to that of the UC fields (blue trace) and TD (dashed orange trace), and 45% smaller than SATD (solid purple trace). Moreover, we find that the RADD RMS value for $\varphi = \pi$ is 25% smaller compared to the RADD RMS value for $\varphi = 0$.

As a consequence of reducing the RMS amplitude, RADD also reduces the overall amplitude of the control fields. To highlight the improvement in the field amplitudes, we compare in Figs. 12(c) and (d) the absolute

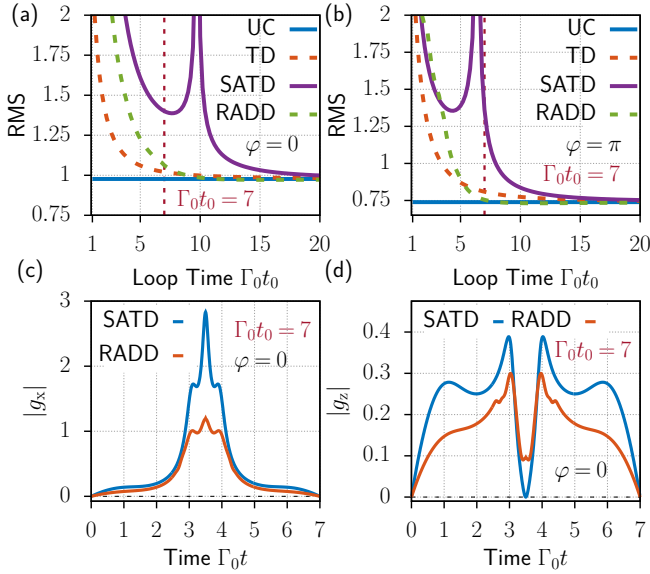


Figure 12. Comparison of resources needed to implement different STAs. (a) RMS amplitude as a function of $\Gamma_0 t_0$ for the circular control loop γ_{circ} [see Eq. (25)] with basepoint at $\varphi = 0$. (b) Similar to (a), but with $\varphi = \pi$. (c) Absolute value of $g_x[i]$ for $i \in \{\mu, \mu_{\text{mod}}\}$ [see Eqs. (38), (33), and (42)] showing the overall improvement in field magnitude for $\Gamma_0 t_0 = 10$ and $\varphi = 0$. (d) Same as (c) but for g_z . In (c), we plotted W_{TD} for comparison [see Eq. (29)].

value of $g_x(t)$ and $g_z(t)$ between RADD (orange trace) and SATD (blue trace) for $\Gamma_0 t_0 = 7$ and $\varphi = 0$, respectively. Our results show that RADD reduces the overall field amplitudes, while yielding low average fidelity errors. For the chosen loop time, $\Gamma_0 t_0 = 7$, we have an average fidelity error of $\langle \mathcal{E}_{-, -} \rangle \lesssim 10^{-3}$ [see Fig. 11(c)], associated to generating the topological defined in Eq. (24).

We stated that $\Gamma_0 t_0 = 7$ is the upper-bound limit for loop times to be robust against parameter imprecisions, but as our results indicate it is also the lower-bound limit that yields control fields with “reasonable” amplitudes. Since the control field amplitude of TD scales like $1/t_0$ [see Eq. (29)] and that of SATD and RADD like $1/t_0^2$ [see Eq. (38)], one cannot arbitrarily shorten the control loop time. This would result in impractical control fields. We surmise this behavior to be linked to the existence of a speed limit akin the quantum speed limit [83].

H. Experimental Realization

We now provide an example of an experimental platform, where our control schemes can be realized.

We consider an optomechanical setup with two laser drives, such that each mechanical mode is coupled to two optical modes [62]. Tracing out the degrees of freedom associated to the optical modes leads to the effective non-

Hermitian Hamiltonian given by

$$\hat{H} = \sum_{j=1}^2 \left(\omega_{\text{mech},j} - i \frac{\gamma_{\text{mech},j}}{2} - i g_j^2 \eta \right) |j\rangle\langle j| - i \eta g_1 g_2 \hat{\sigma}_x. \quad (44)$$

where $\omega_{\text{mech},j}$, $\gamma_{\text{mech},j}$ and g_j are the frequency, damping rate, and optomechanical coupling constant of the j th mechanical mode, respectively. The complex mechanical susceptibility η is given by

$$\eta = \frac{P_L}{\hbar \Omega_{L,j}} \frac{\kappa_{\text{in},j}}{(\kappa/2)^2 + \delta_0^2} \times \left[\frac{1}{\kappa/2 - i(\omega_0 + \delta_0)} - \frac{1}{\kappa/2 + i(-2\omega_0 + \delta_0)} \right], \quad (45)$$

where δ_0 is the mean detuning between the laser and the cavity, κ is the linewidth of the cavity, κ_{in} is the input coupling rate of the cavity, $\omega_0 = (\omega_1 + \omega_2)/2$, P_L is the power of the laser and Ω_L its frequency. Equation (44) can be made time-dependent by making both the power and frequency of the laser time dependent. Within this framework, the effective NH Hamiltonian describing the evolution of the optomechanical setup resembles the two-mode NH Hamiltonian defined in Eq. (12).

By mapping Eq. (44) to $\hat{H}_{\text{sym}}(t) + \hat{H}_{\text{RADD}}(t)$ [see Eqs. (12) and (42)], we can find the modified time-dependent optomechanical NH that allows one to generate the desired braiding operations. This procedure reduces to solving two equations for two unknowns: $P_L(t)$ and $\delta_0(t)$.

IV. CONCLUSION

In this work we have demonstrated how to construct shortcuts-to-adiabaticity for non-Hermitian systems in the presence of spectral singularities. Failing to account for the latter and naively following the recipe developed for Hermitian Hamiltonians will lead to control schemes that do not generate the desired dynamics.

We found that valid NH STAs, in stark contrast to the Hermitian case, do not lead to a family of control schemes characterized by the protocol duration. Besides the fundamental aspect, this has practical implications since a given NH STA may be constrained to long protocol durations. As we have discussed, NH STAs are unstable in this regime in the presence of parameter uncertainties.

The lack of inherent robustness limits the use of celebrated protocols like TD and SATD in realistic settings, but as we have shown the versatility of our approach allows one to find STAs that are robust against parameter uncertainties and constrained in terms of experimental resources. Our results pave the way towards a new class of control protocols, for both classical and quantum systems, that leverage the interplay between coherent and incoherent dynamics.

Appendix A: Criteria for Eigenvalue Braiding

For a two-mode system described by a symmetric NH Hamiltonian, i.e., $\text{Tr}[\hat{H}(t)] = 0$, the following conditions hold true:

$$\begin{aligned} \text{(I)} : \lambda_{\pm}(0) &= \lambda_{\mp}(t_0) = \lambda_{\pm}(2t_0), \\ \text{(II)} : \int_0^{t_0} dt \lambda_{\pm}(t) &\neq 0 \text{ and,} \\ \int_0^{2t_0} dt \lambda_{\pm}(t) &= 0. \end{aligned} \quad (\text{A1})$$

where $\lambda_{\pm}(t)$ are the holomorphic eigenvalues associated to the NH Hamiltonian $\hat{H}(t)$.

Condition (I) expresses the fact that encircling an EP_2 twice with a control loop that results from the concatenation of two loops with the same orientation brings the spectrum back to its original position on the Riemann surface associated to the spectrum of $\hat{H}(t)$.

Condition (II) follows from condition (I) and expresses the fact that encircling an EP_2 twice with a control loop that corresponds to the concatenation of two identical loops leads to $\lambda_{\pm}(t)$, $t \in [0, 2t_0]$, to be an anti-symmetric function with respect to $t = t_0$.

-
- [1] L. Feng, R. El-Ganainy, and L. Ge, Non-hermitian photonics based on parity–time symmetry, *Nature Photonics* **11**, 752 (2017).
- [2] A. Li, H. Wei, M. Cotrufo, W. Chen, S. Mann, X. Ni, B. Xu, J. Chen, J. Wang, S. Fan, C.-W. Qiu, A. Alù, and L. Chen, Exceptional points and non-hermitian photonics at the nanoscale, *Nature Nanotechnology* **18**, 706 (2023).
- [3] M.-A. Miri and A. Alù, Exceptional points in optics and photonics, *Science* **363**, eaar7709 (2019).
- [4] Z. Zhang, D. Ma, J. Sheng, Y. Zhang, Y. Zhang, and M. Xiao, Non-hermitian optics in atomic systems, *Journal of Physics B: Atomic, Molecular and Optical Physics* **51**, 072001 (2018).
- [5] R. Dum, P. Zoller, and H. Ritsch, Monte carlo simulation of the atomic master equation for spontaneous emission, *Phys. Rev. A* **45**, 4879 (1992).
- [6] Y.-C. Wang, J.-S. You, and H. H. Jen, A non-hermitian optical atomic mirror, *Nature Communications* **13**, 4598 (2022).
- [7] A. McDonald, R. Hanai, and A. A. Clerk, Nonequilibrium stationary states of quantum non-hermitian lattice models, *Phys. Rev. B* **105**, 064302 (2022).
- [8] Z. Li, L.-W. Wang, X. Wang, Z.-K. Lin, G. Ma, and J.-H. Jiang, Observation of dynamic non-hermitian skin effects, *Nature Communications* **15**, 6544 (2024).
- [9] X. Li, Y. Cao, and J. Ng, Non-hermitian non-equipartition theory for trapped particles, *Nature Communications* **15**, 1963 (2024).
- [10] K. Ding, C. Fang, and G. Ma, Non-Hermitian topology and exceptional-point geometries, *Nature Reviews Physics* **4**, 745 (2022).
- [11] Y. Ashida, Z. Gong, and M. Ueda, Non-hermitian physics, *Advances in Physics* **69**, 249–435 (2020).
- [12] M. De Carlo, F. De Leonardis, R. A. Soref, L. Colatorti, and V. M. N. Passaro, Non-hermitian sensing in photonics and electronics: A review, *Sensors* **22**, 10.3390/s22113977 (2022).
- [13] C. Wang, Z. Fu, W. Mao, J. Qie, A. D. Stone, and L. Yang, Non-hermitian optics and photonics: from classical to quantum, *Adv. Opt. Photon.* **15**, 442 (2023).
- [14] T. Kato, *Perturbation theory for linear operators; 2nd ed.*, Grundlehren der mathematischen Wissenschaften : a series of comprehensive studies in mathematics (Springer, Berlin, 1976).
- [15] W. D. Heiss, The physics of exceptional points, *Journal of Physics A: Mathematical and Theoretical* **45**, 444016 (2012).
- [16] S. Ozdemir, S. Rotter, F. Nori, and L. Yang, Parity–time symmetry and exceptional points in photonics, *Nature Materials* **18**, 1 (2019).
- [17] N. Okuma and M. Sato, Non-hermitian topological phenomena: A review, *Annual Review of Condensed Matter Physics* **14**, 83 (2023).
- [18] C. Dembowski, H.-D. Gräf, H. L. Harney, A. Heine, W. D. Heiss, H. Rehfeld, and A. Richter, Experimental observation of the topological structure of exceptional points, *Phys. Rev. Lett.* **86**, 787 (2001).
- [19] C. Guria, Q. Zhong, S. K. Ozdemir, Y. S. S. Patil, R. El-Ganainy, and J. G. E. Harris, Resolving the topology of encircling multiple exceptional points, *Nature Communications* **15**, 1369 (2024).
- [20] K. Ding, G. Ma, M. Xiao, Z. Q. Zhang, and C. T. Chan, Emergence, coalescence, and topological properties of multiple exceptional points and their experimental realization, *Phys. Rev. X* **6**, 021007 (2016).
- [21] Y. S. S. Patil, J. Höller, P. A. Henry, C. Guria, Y. Zhang, L. Jiang, N. Kralj, N. Read, and J. G. E. Harris, Measuring the knot of non-Hermitian degeneracies and non-commuting braids, *Nature* **607**, 271 (2022).
- [22] R. Uzdin, A. Mailybaev, and N. Moiseyev, On the observability and asymmetry of adiabatic state flips generated by exceptional points, *Journal of Physics A: Mathematical and Theoretical* **44**, 435302 (2011).
- [23] C. C. Wojcik, K. Wang, A. Dutt, J. Zhong, and S. Fan, Eigenvalue topology of non-hermitian band structures in two and three dimensions, *Physical Review B* **106**, 10.1103/physrevb.106.1161401 (2022).
- [24] M. V. Berry, Quantal phase factors accompanying adiabatic changes, *Proceedings of the Royal Society of London. Series A, Mathematical and Physical Sciences* **392**, 45 (1984).
- [25] Z. Gong, Y. Ashida, K. Kawabata, K. Takasan, S. Higashikawa, and M. Ueda, Topological phases of non-hermitian systems, *Phys. Rev. X* **8**, 031079 (2018).
- [26] A. A. Mailybaev, O. N. Kirillov, and A. P. Seyranian, Geometric phase around exceptional points, *Phys. Rev.*

- A **72**, 014104 (2005).
- [27] S.-D. Liang and G.-Y. Huang, Topological invariance and global berry phase in non-hermitian systems, *Phys. Rev. A* **87**, 012118 (2013).
- [28] W. Liu, Y. Wu, C.-K. Duan, X. Rong, and J. Du, Dynamically encircling an exceptional point in a real quantum system, *Phys. Rev. Lett.* **126**, 170506 (2021).
- [29] J. Doppler, A. A. Mailybaev, J. Böhm, U. Kuhl, A. Girschik, F. Libisch, T. J. Milburn, P. Rabl, N. Moiseyev, and S. Rotter, Dynamically encircling an exceptional point for asymmetric mode switching, *Nature* **537**, 76–79 (2016).
- [30] W. Chen, M. Abbasi, Y. N. Joglekar, and K. W. Murch, Quantum jumps in the non-hermitian dynamics of a superconducting qubit, *Phys. Rev. Lett.* **127**, 140504 (2021).
- [31] H. Wang, L.-J. Lang, and Y. D. Chong, Non-hermitian dynamics of slowly varying hamiltonians, *Phys. Rev. A* **98**, 012119 (2018).
- [32] G. Nenciu and G. Rasche, On the adiabatic theorem for nonself-adjoint hamiltonians, *Journal of Physics A: Mathematical and General* **25**, 5741 (1992).
- [33] N. Moiseyev, *Non-Hermitian Quantum Mechanics* (Cambridge University Press, 2011).
- [34] T. Kato, On the adiabatic theorem of quantum mechanics, *Journal of the Physical Society of Japan* **5**, 435 (1950).
- [35] M. V. Berry and R. Uzdin, Slow non-hermitian cycling: exact solutions and the stokes phenomenon, *Journal of Physics A: Mathematical and Theoretical* **44**, 435303 (2011).
- [36] M. Maamache, *Non-unitary evolution of quantum time-dependent non-hermitian systems* (2017).
- [37] M. Demirplak and S. A. Rice, Adiabatic population transfer with control fields, *The Journal of Physical Chemistry A* **107**, 9937 (2003).
- [38] M. Demirplak and S. Rice, On the consistency, extremal, and global properties of counterdiabatic fields, *The Journal of chemical physics* **129**, 154111 (2008).
- [39] M. Berry, Transitionless quantum driving, *Journal of Physics A: Mathematical and Theoretical* **42**, 365303 (2009).
- [40] D. Guéry-Odelin, A. Ruschhaupt, A. Kiely, E. Torrontegui, S. Martínez-Garaot, and J. G. Muga, Shortcuts to adiabaticity: Concepts, methods, and applications, *Rev. Mod. Phys.* **91**, 045001 (2019).
- [41] T. Hatomura, Shortcuts to adiabaticity: theoretical framework, relations between different methods, and versatile approximations, *Journal of Physics B: Atomic, Molecular and Optical Physics* **57**, 102001 (2024).
- [42] S. Ibáñez, X. Chen, E. Torrontegui, J. G. Muga, and A. Ruschhaupt, Multiple schrödinger pictures and dynamics in shortcuts to adiabaticity, *Phys. Rev. Lett.* **109**, 100403 (2012).
- [43] A. Baksic, H. Ribeiro, and A. A. Clerk, Speeding up adiabatic quantum state transfer by using dressed states, *Phys. Rev. Lett.* **116**, 230503 (2016).
- [44] B. B. Zhou, A. Baksic, H. Ribeiro, C. G. Yale, F. J. Heremans, P. C. Jerger, A. Auer, G. Burkard, A. A. Clerk, and D. D. Awschalom, Accelerated quantum control using superadiabatic dynamics in a solid-state lambda system, *Nature Physics* **13**, 330 (2017).
- [45] S. Ibáñez, S. Martínez-Garaot, X. Chen, E. Torrontegui, and J. G. Muga, Shortcuts to adiabaticity for non-hermitian systems, *Phys. Rev. A* **84**, 023415 (2011).
- [46] B. T. Torosov, G. Della Valle, and S. Longhi, Non-hermitian shortcut to adiabaticity, *Phys. Rev. A* **87**, 052502 (2013).
- [47] H. Ribeiro and F. Marquardt, Accelerated non-reciprocal transfer of energy around an exceptional point, *arXiv* (2021).
- [48] I. I. Arkhipov, F. Minganti, A. Miranowicz, i. m. c. K. Özdemir, and F. Nori, Restoring adiabatic state transfer in time-modulated non-hermitian systems, *Phys. Rev. Lett.* **133**, 113802 (2024).
- [49] Q.-C. Wu, J.-L. Zhao, Y.-H. Zhou, B.-L. Ye, Y.-L. Fang, Z.-W. Zhou, and C.-P. Yang, Shortcuts to adiabatic state transfer in time-modulated two-level non-Hermitian systems, *arXiv e-prints*, arXiv:2411.00428 (2024).
- [50] R. Gilmore, *Catastrophe Theory for Scientists and Engineers* (Wiley, 2007).
- [51] C. M. Bender and S. Boettcher, Real spectra in non-hermitian hamiltonians having pt symmetry, *Phys. Rev. Lett.* **80**, 5243 (1998).
- [52] K. Ding, Z. Q. Zhang, and C. T. Chan, Coalescence of exceptional points and phase diagrams for one-dimensional P T -symmetric photonic crystals, *Phys. Rev. B* **92**, 235310 (2015).
- [53] F. Klauck, L. Teuber, M. Ornigotti, M. Heinrich, S. Scheel, and A. Szameit, Observation of pt-symmetric quantum interference, *Nature Photonics* **13**, 883–887 (2019).
- [54] S.-Y. Lee, J.-W. Ryu, S. W. Kim, and Y. Chung, Geometric phase around multiple exceptional points, *Phys. Rev. A* **85**, 064103 (2012).
- [55] G. Demange and E.-M. Graefe, Signatures of three coalescing eigenfunctions, *Journal of Physics A: Mathematical and Theoretical* **45**, 025303 (2011).
- [56] E. M. Graefe, U. Günther, H. J. Korsch, and A. E. Niederle, A non-hermitian symmetric bose-hubbard model: eigenvalue rings from unfolding higher-order exceptional points, *Journal of Physics A: Mathematical and Theoretical* **41**, 255206 (2008).
- [57] J.-W. Ryu, S.-Y. Lee, and S. W. Kim, Analysis of multiple exceptional points related to three interacting eigenmodes in a non-hermitian hamiltonian, *Phys. Rev. A* **85**, 042101 (2012).
- [58] A. Hatcher, *Algebraic Topology* (Cambridge University Press, Cambridge, 2002).
- [59] W. D. Heiss, Repulsion of resonance states and exceptional points, *Phys. Rev. E* **61**, 929 (2000).
- [60] M. V. Berry and D. H. J. O’Dell, Diffraction by volume gratings with imaginary potentials, *Journal of Physics A: Mathematical and General* **31**, 2093 (1998).
- [61] E. Artin, Theory of braids, *Annals of Mathematics* **48**, 101 (1947).
- [62] H. Xu, D. Mason, L. Jiang, and J. Harris, Topological energy transfer in an optomechanical system with exceptional points, *Nature* **537**, 80 (2016).
- [63] G. Nenciu, On the adiabatic theorem of quantum mechanics, *Journal of Physics A: Mathematical and General* **13**, L15 (1980).
- [64] Q. Zhong, M. Khajavikhan, D. N. Christodoulides, and R. El-Ganainy, Winding around non-hermitian singularities, *Nature* **9**, 4808 (2018).
- [65] T. Dai, Y. Ao, J. Mao, Y. Yang, Y. Zheng, C. Zhai, Y. Li, J. Yuan, B. Tang, Z. Li, J. Luo, W. Wang, X. Hu,

- Q. Gong, and J. Wang, Non-hermitian topological phase transitions controlled by nonlinearity, *Nature* **20**, 101 (2024).
- [66] R. El-Ganainy, K. G. Makris, M. Khajavikhan, Z. H. Musslimani, S. Rotter, and D. N. Christodoulides, Non-hermitian physics and \mathcal{PT} symmetry, *Nature* **14**, 11 (2018).
- [67] J. Yang, S. Shi, S. Yan, R. Zhu, X. Zhao, Y. Qin, B. Fu, X. Chen, H. Li, Z. Zuo, K. Jin, Q. Gong, and X. Xu, Non-orthogonal cavity modes near exceptional points in the far field, *Communications Physics* **7**, 13 (2024).
- [68] J. del Pino, J. J. Slim, and E. Verhagen, Publisher correction: Non-hermitian chiral phononics through optomechanically induced squeezing, *Nature* **611**, E11 (2022).
- [69] H.-K. Lau and A. A. Clerk, Fundamental limits and non-reciprocal approaches in non-hermitian quantum sensing, *Nature Communications* **9**, 4320 (2018).
- [70] L. Huang, S. Huang, C. Shen, S. Yves, A. S. Pilipchuk, X. Ni, S. Kim, Y. K. Chiang, D. A. Powell, J. Zhu, Y. Cheng, Y. Li, A. F. Sadreev, A. Alù, and A. E. Miroshnichenko, Acoustic resonances in non-hermitian open systems, *Nature Reviews Physics* **6**, 11 (2024).
- [71] J. W. Brown and R. V. Churchill, *Complex Variables and Applications*, eighth ed. (McGraw-Hill Higher Education, Boston, MA, 2009).
- [72] A. Wilkey, J. Suelzer, Y. N. Joglekar, and G. Vemuri, Theoretical and experimental characterization of non-markovian anti-parity-time systems, *Communications Physics* **6**, 308 (2023).
- [73] W. Chen, Ş. Kaya Özdemir, G. Zhao, J. Wiersig, and L. Yang, Exceptional points enhance sensing in an optical microcavity, *Nature* **548**, 192 (2017).
- [74] K. Y. Bliokh, D. Leykam, M. Lein, and F. Nori, Topological non-hermitian origin of surface maxwell waves, *Nature Communications* **10**, 580 (2019).
- [75] L. V. Ahlfors and L. Sario, *Riemann Surfaces*, Princeton Mathematical Series, Vol. 26 (Princeton University Press, Princeton, NJ, 1960) pp. xi+382.
- [76] M. Ornigotti and A. Szameit, Quasi \mathcal{PT} -symmetry in passive photonic lattices, *Journal of Optics* **16**, 065501 (2014).
- [77] S. Scheel and A. Szameit, \mathcal{PT} -symmetric photonic quantum systems with gain and loss do not exist, *EPL (Europhysics Letters)* **122**, 34001 (2018).
- [78] A. Guo, G. J. Salamo, D. Duchesne, R. Morandotti, M. Volatier-Ravat, V. Aimez, G. A. Siviloglou, and D. N. Christodoulides, Observation of \mathcal{PT} -symmetry breaking in complex optical potentials, *Phys. Rev. Lett.* **103**, 093902 (2009).
- [79] P. K. Ghosh, Classical hamiltonian systems with balanced loss and gain, *Journal of Physics: Conference Series* **2038**, 012012 (2021).
- [80] Q.-C. Wu, Y.-L. Fang, Y.-H. Zhou, J.-L. Zhao, Y.-H. Kang, Q.-P. Su, and C.-P. Yang, Efficient symmetric and asymmetric bell-state transfers in a dissipative jaynes-cummings model, *arXiv preprint arXiv:2411.10812* (2024).
- [81] M. G. Bason, M. Viteau, N. Malossi, P. Huillery, E. Arimondo, D. Ciampini, R. Fazio, V. Giovannetti, R. Manella, and O. Morsch, High-fidelity quantum driving, *Nature Physics* **8**, 147 (2012).
- [82] X. Chen, E. Torrontegui, and J. G. Muga, Lewis-riesenfeld invariants and transitionless quantum driving, *Phys. Rev. A* **83**, 062116 (2011).
- [83] L. Mandelstam and I. Tamm, The uncertainty relation between energy and time in non-relativistic quantum mechanics, in *Selected Papers*, edited by B. M. Bolotovskii, V. Y. Frenkel, and R. Peierls (Springer Berlin Heidelberg, Berlin, Heidelberg, 1991) pp. 115–123.